Supramolecular nanotechnology: from molecules to devices

Henrique E. Toma

Instituto de Quimica, Universidade de São Paulo, Caixa Postal 26077 CEP 05513-970 São Paulo, Brazil

Supramolecular chemistry, also known as the chemistry beyond the molecules, provides the best route for molecular nanotechnology, allowing the design of versatile functional nanomaterials conveying the remarkable characteristics of the molecular centers, including their electronic, optical and chemical properties. Synthetic strategies have been successfully developed for the assembly of supramolecular systems encompassing porphyrins, porphyrazines, clusters and polyimine complexes. Their many applications in nanotechnological devices, such as amperometric sensors, smart windows, photoelectrochemical cells and logic gates are dealt with in this article.

Keywords: Amperometric sensors, molecular devices, molecular nanotechnology, molecular logic gates, supramolecular chemistry.

Introduction

SUPRAMOLECULAR[1,2] chemistry provides a powerful tool for assembling complex molecular systems exhibiting functionality or mimicking biological systems in their organization, cooperative functions, energy conversion and information storage. For this purpose, molecular entities displaying suitable properties should be connected by appropriate groups in order to transmit information and provide adequate interaction between them[1–3]. This can be done by means of hydrogen bonding, dipole–dipole and van der Waals interactions, as well as, by forming coordination bonds. Such intermolecular interactions can be rather strong, as observed in π-stacked porphyrins and pthalocyanines. Another interesting way of getting supramolecular structures is by self-assembling weakly interacting species such as amphiphilic molecules, as observed in membranes, vesicles and Langmuir–Blodgett (LB) films.

A supramolecular system exhibits structural and active components. The last ones are responsible for performing some action and promoting functionality when put together in an organized way, e.g. by forming and breaking chemical bonds, absorbing or emitting light, transferring electron or energy, etc. The structural components are necessary for assembling and connecting the components in an organized way, in order to get molecular recogni-

tion, allosteric effects, or to provide energy gradients for promoting directional processes.

In this way, molecular devices can be inspired on a supramolecular approach in which the components are functionally integrated to execute an action or process[1,2]. A simple design consists of a molecular film inserted into a pair of optical or conducting windows; however, molecular devices can also be assembled into very complex ways in analogy with the electronic devices[4–8].

In the supramolecular design, the use of metal–ligand interactions has many advantages, since it can be guided by the self-assembly character of the metal–ligand interaction, allowing the selectivity control based on simple acid-base principles, while incorporating a variety of structural, electronic and kinetic properties from the molecular systems. Metal complexes can be kinetically labile or inert and their structures can exhibit many different coordination numbers and geometries (trigonal, square, pyramidal, octahedral, capped octahedral, pentagonal bipyramidal, etc.), depending on the element and its oxidation state. In this way, the coordination chemistry-based approach can be employed in metal ion induced assembly of highly organized structures, as those obtained from the direct interaction between linear polypyridine polymers and copper(I) ions[1]. Many transition metal complexes can be used for this purpose, but the ruthenium[3,9–13], palladium or platinum[14,15] compounds have been most commonly employed.

This article will focus on the supramolecular assembly of symmetric coordination compounds exhibiting several strategically distributed binding sites, as illustrated in Figure 1[3,16,17]. Those molecular building blocks allow to build up a variety of linear, planar or tridimensional systems, incorporating or combining relevant physico-chemical properties for application in nanotechnological devices.
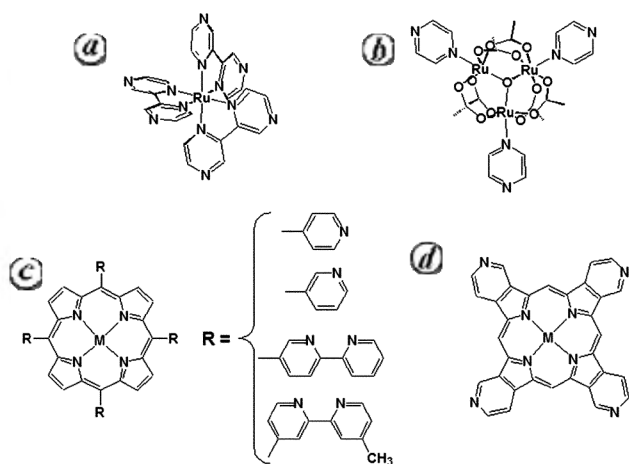
In the representative examples of Figure 1, the tris-(2,2'-bipyrazine)ruthenium(II) complex (a) belongs to the class of ruthenium(II) polyimines which are among the most extensively investigated compounds in the last decades, because of their remarkable photochemical, photophysical and redox properties[18–26]. The available six coordinating pyrazine N-atoms in an octahedral arrangement can be directly used to build up supramolecular systems in the presence of metal ions. Additional bridging ligands (BL) can also be added, yielding mixed complexes of the type $[Ru(bipy)(BL)_2]$ and $[Ru(bipy)_2(BL)]$

e-mail: henetoma@iq.usp.br

(bipy = 2,2′-bipyridine) which can be useful for assembling new polynuclear systems. In fact, Balzani *et al.*[27] have already employed this strategy focusing on 'complex as metals and complex as ligands', for developing a number of interesting supramolecular systems.

Another important class of complexes shown in Figure 1 *b*, consists of triangular *μ*-oxo-bridged ruthenium-acetate clusters[23,40–75]. Their main characteristics are the strong electronic delocalization and the occurrence of five successive monoelectronic redox processes in the range of −2.0 to 2.0 V. The electronic properties of the triangular μ-ORu$_3$ center are modulated by the nature of the axial ligands, allowing the fine tuning of the redox potentials. Since the electronic effects and the donor/acceptor characteristics are strongly dependent on the oxidation state, contrasting redox species can be readily produced by changing the applied potentials. In fact, by applying negative potentials the triangular clusters become stronger π-donor species, while by reversing the potentials, they acquire strong π-acceptor characteristics. Because of their robust, symmetric structures, these triangular clusters provide versatile building blocks for generating structures connected by suitable bridging ligands such as pyrazine (pz) and 4,4′-bipyridine (4,4′bipy).

The next relevant system shown in Figure 1 corresponds to porphyrins, metalloporphyrins and related macrocycles[3,16,17]. Porphyrins are particularly important prosthetic groups in biological systems, acting as the active sites in many different biomolecules, particularly cytochromes, electron-transfer cofactors, oxygen transport and storage (hemoglobin and myoglobin) and photochemically active site in the photosynthetic system. These species exhibit planar and relatively rigid structures suitable for the preparation of materials displaying cavities or that can self-assemble by electrostatic and π–π interactions. They

also provide interesting functional building-blocks because of their rich coordination, catalytic, electrocatalytic, photochemical and redox properties, as described earlier[3,16,17,28–36]. In addition to the extended aromatic macrocyclic structure, there is a rich coordination chemistry associated with the presence of four inner ring nitrogen atoms. The free-base and metallated *meso*-tetra(4-pyridyl)porphyrins (M-TPyP, Figure 1 *d*) can combine with several metal complexes through the bridging pyridine ligand at the four meso-positions of the porphyrin, allowing to build up interesting biomimetic systems[13,37–53].

The last system in Figure 2 *d* corresponds to the tetra-pyridylporphyrazines (M-TPyPz). Because the pyridine rings are fused to the beta-pyrrolic sites, they are more closely related to the class of phtalocyanine compounds[54–56].

The multibridging complexes shown in Figure 1 can be interconnected by using suitable transition metal ions as linking elements. However, specific synthetic methodology should be developed to build up more complicated architectures. An example is the convergent synthetic approach illustrated in Figure 2, for the generation of cluster dendrimers[17,57–76].

Figure 2. Illustration of a three step convergent synthetic approach, starting from triangular building blocks for the generation of a dendrimeric cluster encompassing 30 ruthenium atoms.
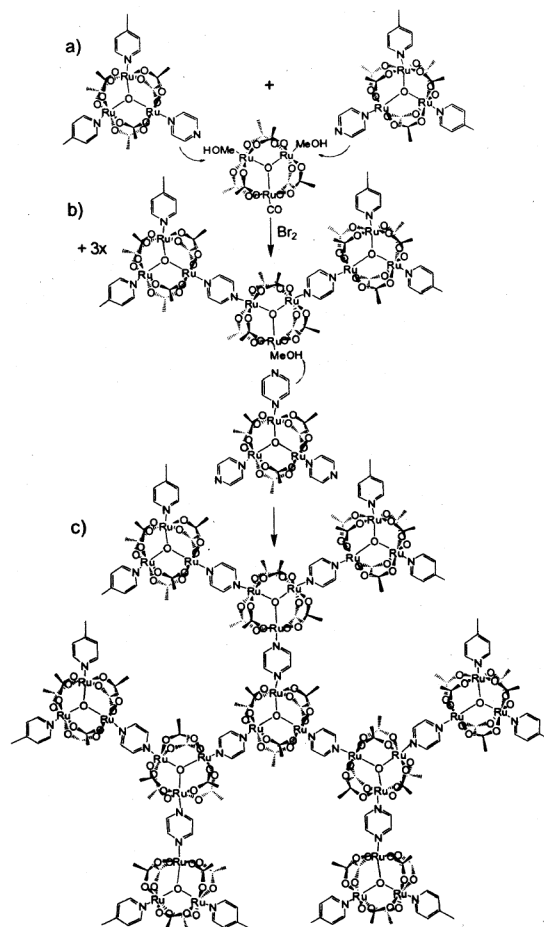

Figure 1. Typical metal-organic building-blocks constituted by metal polyimines (*a*), metal clusters (*b*), porphyrins (*c*) and porphyrazines (*d*), which can be employed in the assembly of functional supramolecular nanomaterials, based on the coordination chemistry approach.

Metal complexes can also be attached to multibridging core species, performing as the ending elements. However, by choosing convenient ancillary complexes, one can also introduce functional groups for selective molecular interactions or for carrying out electrochemical coupling via electropolymerization reactions[13,47,53]. In fact, a great variety of interesting supermolecules has been obtained by attaching transition metal complexes such as ruthenium-polypyridines, ruthenium-edta, pentacyanoferrate and trinuclear μ_3-ORu$_3$(OAc)$_6$ clusters to the peripheral pyridyl groups of metallated meso-tetra(pyridyl)porphyrins (Figure 3). In such systems, the peripheral complexes R can play many roles[3]. For instance, they can modify the local environment around the porphyrin ring and exert protection effects against radicals and other highly reactive species. In addition, they can improve solvation and solubility properties, or act as cofactor in redox processes. As tunable electron donor–acceptor groups, they can induce electronic effects on the metalloporphyrin center. Finally, they can provide important sites for intra- and/or intermolecular interactions, favouring the assembly of supramolecular structures and materials and the occurrence of supramolecular interactions.

An important aspect is the facility of those supramolecular species to form films, even by simple methods such as dip-coating and drop casting, thus providing versatile interfaces for many nanotechnological applications.

Among the several species shown in Figure 3, two special classes of compounds have been systematically studied[3,16,17], consisting of tetrasubstituted pyridylporphyrins coordinated with four ruthenium-polypyridines (here de-

noted tetraruthenated pyridylporphyrin, TRPyP) or triangular ruthenium clusters (here denoted tetracluster pyridylporphyrin, TCPyP), (Figure 4).

A related supramolecular species (here denoted TRPyPz = tetraruthenated porphyrazine) is constituted by the (3,4-pyridyl)porphyrazine center coordinated to four peripheral [Ru(bipy)$_2$Cl]$^+$ groups (Figure 5). In this system, the pyridyl groups are fused to the macrocycle ring, in contrast with the related meso-tetra(pyridyl)porphyrins, TPyP,[3] allowing a stronger electronic interaction between the central and peripheral complexes.

Another relevant species is represented by [H$_2$(4-TPyP){Ru(5-Clphen)$_2$Cl}$_4$]$^{4+}$ where 5-Clphen = 5-chlorophenantroline. This species has been denoted electropolymerizable tetraruthenated porphyrin, H$_2$(ETRPyP)[13,47,53,77].

The UV-vis spectra of the TRPyP species can be exemplified by the H$_2$(TRPyP) case. It exhibits the porphyrin Soret and the four Q bands at 414, 518, 560, 584 and 642 nm respectively; and the bands of peripheral complexes at 292 (bipy $\pi \to \pi^*$), 356 [MLCT2 Ru^{II}(dπ) $\to$ bipy(π^*_2)] and ~ 470 nm [MLCT1 Ru^{II}(dπ) $\to$ bipy(π^*_1)] (MLCT = metal to ligand charge transfer). The protonation of the porphyrin ring (pK$_a \cong 2.0$) shifts the Soret band to 440 nm, giving rise to a new band at 690 nm[40] ascribed to a Ru^{II}(dπ)$\to$H$_4$(4-TPyP)(π^*_1) charge transfer transition.

The electronic spectra of a M(TCPyP) complex exhibit electronic transitions in the porphyrin center very similar to those observed in the spectra of the M(TRPyP) species[17,45,51,78–80]. The Soret band is typically in the range of 414–475 nm, and the Q$_{1-0}$ and Q$_{0-0}$ bands in the range of 557–584 and 611–645 nm respectively. In the formal Ru^{III}Ru^{III}Ru^{III} oxidation state, the characteristic intracluster band is observed in the 685–707 range, while the Ru$_3$O$\to$py MLCT band is found in the 314–351 nm range.

Typical cyclic voltammograms of the TRPyP complexes can be seen in Figure 6. The Ru(III/II) redox processes associated with the peripheral ruthenium complexes are responsible for a reversible wave around 0.9 V, exhibiting four times the intensity of those waves centered in the metalloporphyrin moiety[41,46,81,82]. This process is followed by an oxidation wave of the metalloporphyrin above 1.2 V. At negative potentials, two successive monoelectronic waves corresponding to the reduction of the porphyrin to the radical anion (–0.7 V) and the dianion species (–1.1 V) can be observed, followed by the first and second reduction of the bipy-ligands at –1.4 and 1.6 V respectively. In the case of the Co(III), Fe(III) and Mn(III) porphyrins, the reduction to the respective M(II)TPyP species is also possible. Normally, the Co(III/II)TPyP wave is not observed in the cyclic voltammograms because of its slow kinetics, but it is expected around 0.1 V, by analogy with other meso-substituted cobalt porphyrins. On the other hand, the Fe(III)TPyP de-
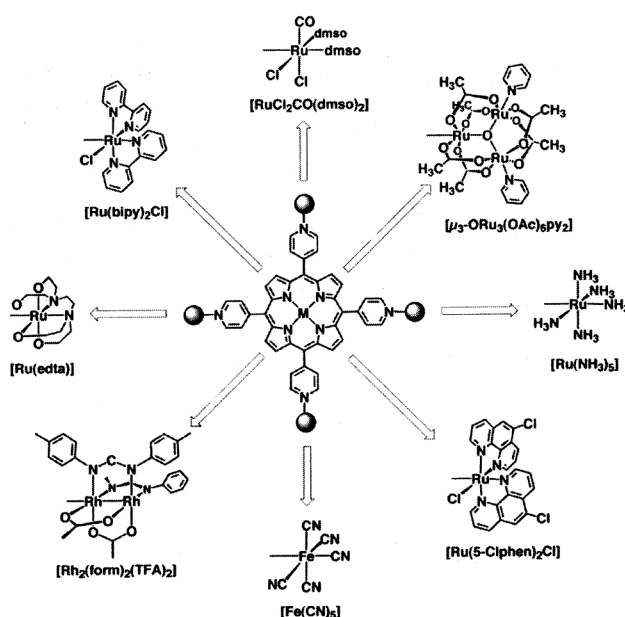
Figure 3. Supramolecular porphyrins obtained by coordination of transition metal complexes to the periphery of the macrocyclic ring (a similar scheme can be extended to the 3-TPyP and analogous porphyrazine species).
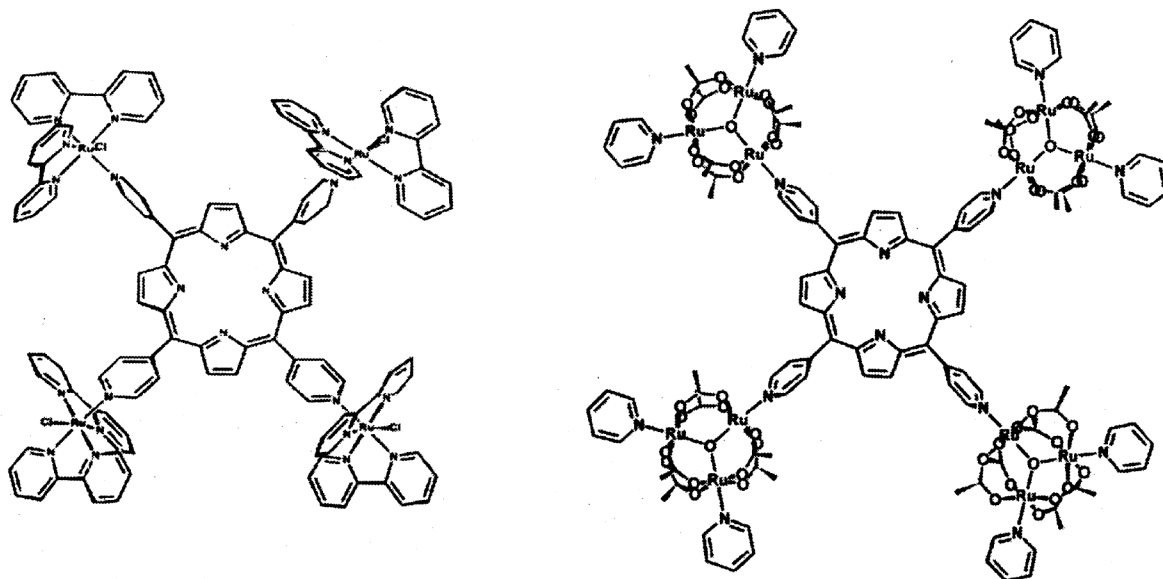
Figure 4. Structural representation of the *meso*-tetrapyridylporphyrin center (central protons omitted for clarity) coordinated to four peripheral [Ru(bipy)$_2$Cl]$^+$ groups, 4-TRPyP (left) and four [μ_3-ORu$_3$(OAc)$_6$(py)$_2$]$^+$ clusters, 4-TCPyP (right) (a similar scheme applies for the 3-TRPyP and 3-TCPyP analogues).
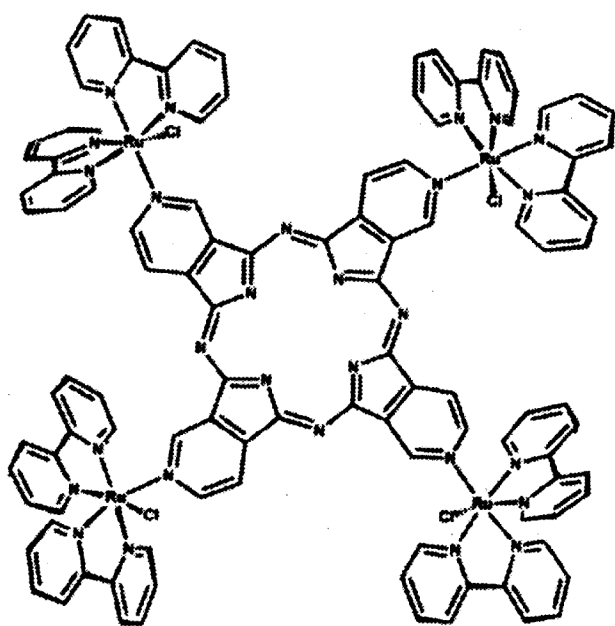
Figure 5. Structural representation of the 3,4-pyridyl)porphyrazine center (central protons omitted for clarity) coordinated to four peripheral [Ru(bipy)$_2$Cl]$^+$ groups (TRPyPz).

rivative tends to form the μ-O(Fe^{III}TPyP)$_2$ dimer, which rapidly dissociates after the reduction step at –0.76 V[83].

The porphyrin reduction potential is also sensitive to the coordinated metal ion and its oxidation state. For example, the reduction of the Co^{II}(4-TRPyP) species is cathodically shifted due to the prior formation of Co^I(4-TRPyP), while the ring oxidation potentials remain al-

most invariant at 1.5 V. Although the M^{I}P state has been reported for Ni, Co and Fe porphyrins, the only case detected in supramolecular porphyrins is for Co^I(4-TRPyP) and Co^I(4-TCPyP), around –1.1 V[45]. Its formation usually shifts the porphyrin and bipy reduction to more negative potentials. In all cases, the spectroelectrochemistry technique has proved essential for the proper assignment of the redox processes (a typical set is shown in Figure 6)[16,38,39,45].

The voltammograms of the M(TCPyP) species are dominated by the [μ_3-ORu$_3$(OAc)$_6$(py)$_2$] reversible waves, as shown in Figure 7. It should be noticed that in the case of [μ_3-ORu$_3$(OAc)$_6$(py)$_3$] and analogous complexes the electronic coupling[17] is close to the strong limit, so that the redox sites are oxidized or reduced at rather contrasting potentials, i.e. separated from each other by ΔE ~1 V[45,78–80]. The porphyrin waves are generally hidden, and can only be found with the aid of spectroelectrochemistry.

In the cyclic voltammograms of Co(4-TCPyP) in Figure 7 *a*, the waves at 1.2 and 2.1 V have been assigned to the consecutive monoelectronic oxidations of the peripheral ruthenium clusters (Figure 7 *b*), and no evidence of Co^{III}P moiety oxidation has been found up to 2.0 V. Although the wave at 0.2 V looks like a conventional cluster wave, the spectroelectrochemistry in the 0.7–0.0 V region revealed the presence of a hidden Co$^{III/II}$P process. By changing the potential from 0.7 to 0.20 V, the Soret and Q bands shift from 435 and 537 nm to 412 and 533 nm respectively, while the ruthenium cluster bands remain the same (Figure 7 *c*). In contrast, by changing the potential from 0.25 to 0.0 V the broad Ru-cluster band at 700 nm shifts to 913 nm, but the porphyrin bands are
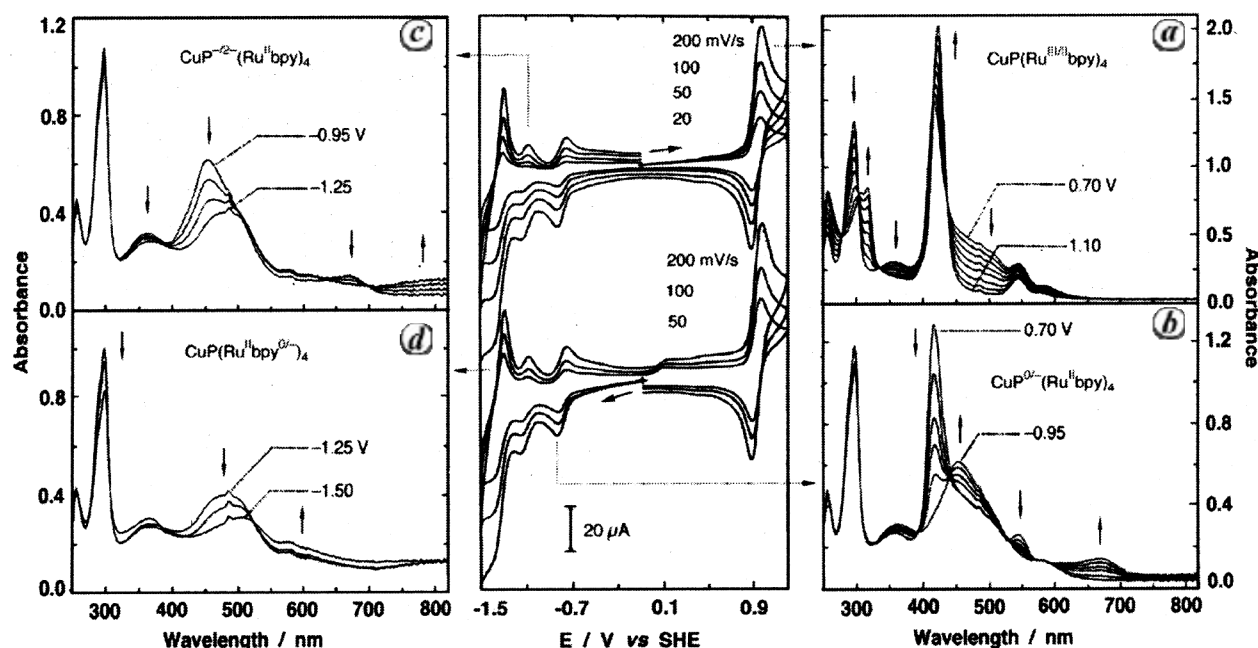
Figure 6. Cyclic voltammograms of [Cu(4-TRPyP)]$^{4+}$ 2.5 mM (center) and the corresponding spectroelectrochemical changes in the range: (*a*) 0.70 to 1.10 V, (*b*) 0.70 to –0.95 V, (*c*) –0.95 to –1.25 V and (*d*) –1.25 to –1.50 V; SHE, in DMF solution.
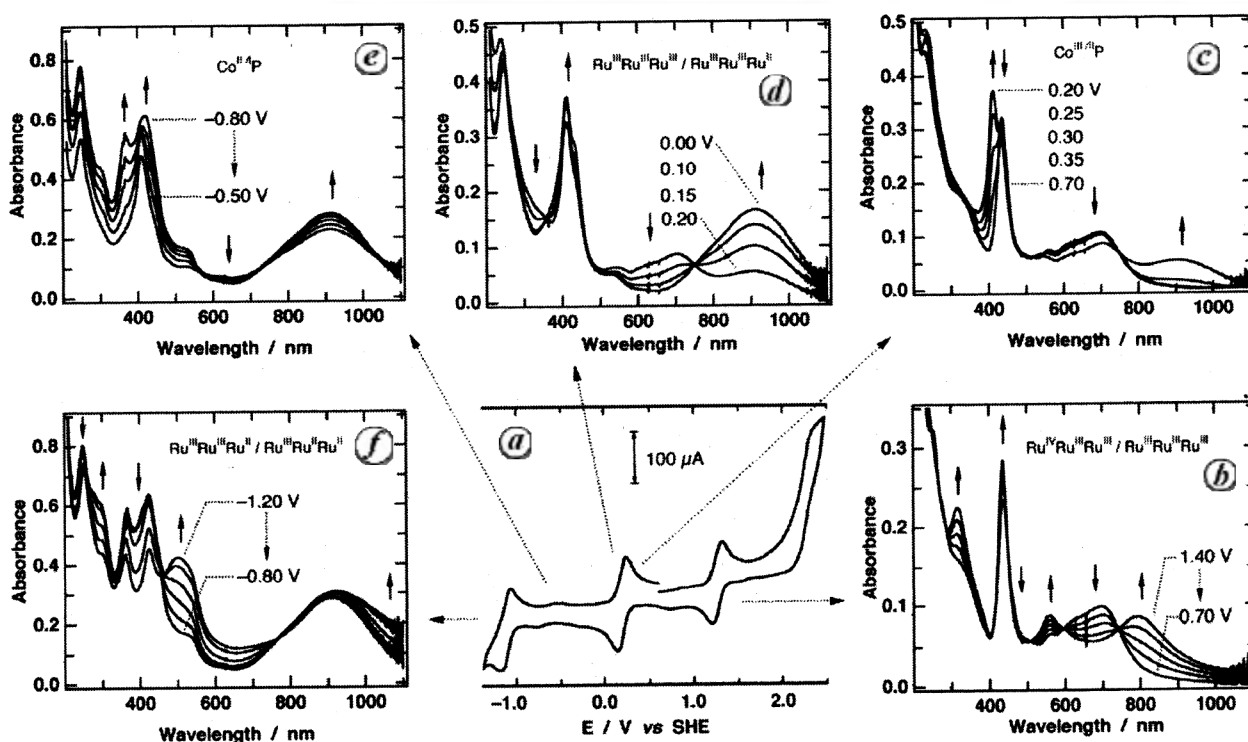
Figure 7. (*a*) Cyclic voltammograms a 3.0 × 10^{-4} M Co(4-TCPyP) in the –1.5 to 2.5 V vs SHE range and the corresponding spectroelectrochemical changes in the (*b*) 0.7–1.4 V, (*c*) 0.2–0.7 V, (*d*) 0.0–0.2 V, (*e*) –0.5 to –0.8 V and (*f*) –0.8 to –1.2 V range, in CH$_3$CN solution.

only slightly perturbed (Figure 7 *d*). The redox potential of the Ru$_3$^{III,III,III}/Ru$_3$^{III,III,II} couple (0.16 V) has been obtained from the spectroelectrochemistry data at 913 nm. The Co$^{III/II}$P potential (0.31 V) has been determined in a

similar way by monitoring the Soret band at 412 nm[45]. Moving to a more negative region, the weak waves at –0.65 V reveal an enhancement of the 913 nm band and of the absorbance below 550 nm, and in addition, new

bands appear at 366 and 300 nm while the Soret band is broadened and shifted from 412 to 421 nm (Figure 7 e). This behaviour is completely different from that expected for the reduction of the porphyrin ring or the peripheral ruthenium clusters and has been assigned to the $Co^{II/I}P$ process. The double Soret band of the Co^IP species becomes more evident when the ruthenium clusters are further reduced to the $Ru_3^{III,II,II}$ species (−0.8 to −1.2 V range), shifting the MLCT band from 400 nm to 502 nm and the intracluster band from 913 to 938 nm (Figure 7 f).

An interesting property of Co–4TPyP is its ability to self-adjust its chemical potential to that of the environment, as illustrated in Figure 8. In this way, it behaves as reducing agent capable of performing, at suitable negative potentials, the electrocatalytical four electrons reduction of dioxygen to water, mimetizing the cytochrome-c oxidase enzyme[45,51]. Under oxidizing conditions, it promotes efficient and selective oxidation of cycloalkanes and other organic substrates, thus mimetizing cytochrome P-450 (refs 12, 52). The peripheral complexes can also act as catalyst cofactors, storing redox equivalents and acting as electron transfer relays in multi-electronic redox processes[3]. Those characteristics are not found in conventional catalysts.

Supramolecular films

Direct assembly

One of the most interesting properties of the M(TRPyP) and M(TCPyP) compounds is their ability to form homogeneous thin films by direct self-assembly based on dip-coating, spray coating, drop-casting or electrostatic assembly procedures[45,56,77,78,81,83–86]. In addition, the films exhibit an important peculiarity: they preserve most of
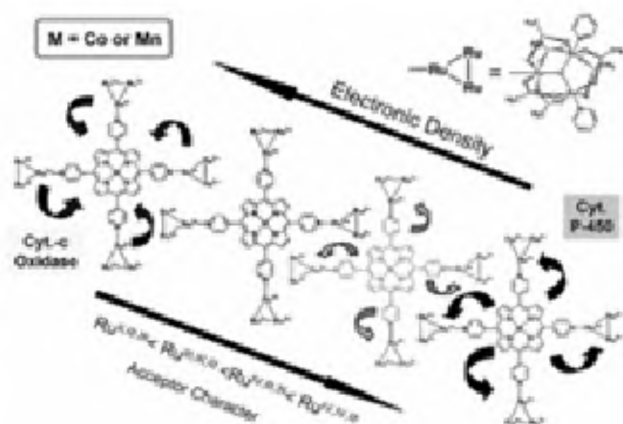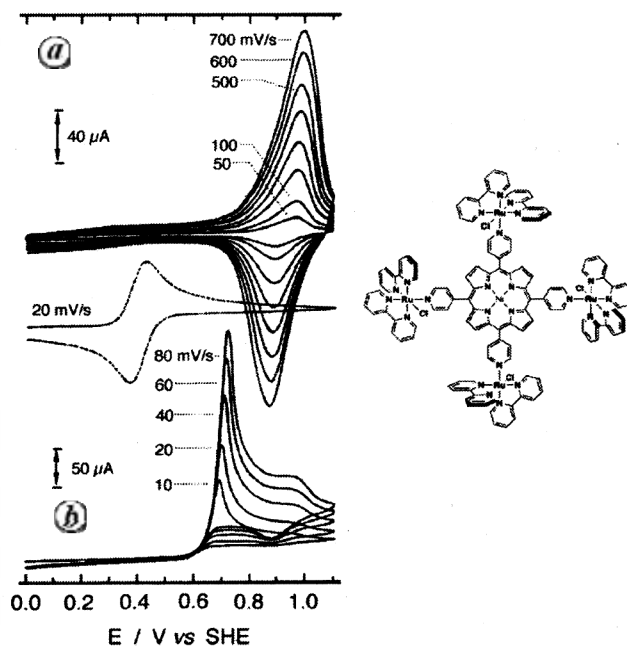
the characteristics of the supramolecular species. For this reason, they provide interesting interfaces for applications in molecular devices. This remarkable point exhibited by M(TRPyP) and M(TCPyP) allows to extend their usefulness as functional materials encompassing a broad range of possibilities not found in most supramolecular systems.

In general, porphyrins exhibit a self-association tendency due to the π–π stacking interactions. This is also observed in the supramolecular species, contributing to the formation of very stable thin films. It should be noticed that the films exhibit excellent optical and electrochemical performance. Even rough films obtained by drop casting $[M(TRPyP)]X_4$ or $[M(TCPyP)]X_4 (X = PF_6^-, ClO_4, CF_3SO_3^-)$ solutions onto glass, exhibit good transparency. Another important point is their strong adherence to most surfaces, including glass, oxides, glassy carbon, graphite, silicon and metals. Although some of the films are slightly soluble in water, their dissolution can be prevented by adding some excess of X^- counter ions into the solution.

The $[M(TRPyP)]X_4$ films exhibit a characteristic pair of sine-shaped waves at $E_{pc} = 0.92$ and $E_{pa} = 0.99$ V (20 Mv s^{-1})[41,81,84] associated with the $Ru^{III/II}$ redox couple, as shown in Figure 9. At this potential, their conductivity becomes very high. The charge-diffusion constant has been estimated to be $D_{CT}^{1/2}C = 1.0 \times 10^{-8}$ mol cm^{-2} s$^{-1/2}$ from the Cottrell plots.

In the presence of ferrocyanide ions[81,84], as one can see in Figure 9, there is no evidence for its characteristic

Figure 8. Redox modulation of the M(TCPyP) catalytic activity by changing the oxidation state of the $[\mu\text{-}ORu_3(CH_3CO_2)_6(py)_2]^+$ complexes in order to perform cytochrome C-oxidase and cytochrome P-450 reactions.

Figure 9. *a*, Cyclic voltamograms of a platinum electrode coated with a $[Ni(4\text{-}TRPyP)][PF_6]_4$ film, recorded in aqueous solution at several potential scan rates. *b*, Comparison of the voltammetric response for $[Fe(CN)_6]^{4-}$ ions, using a bare (middle) and a coated electrode (bottom).
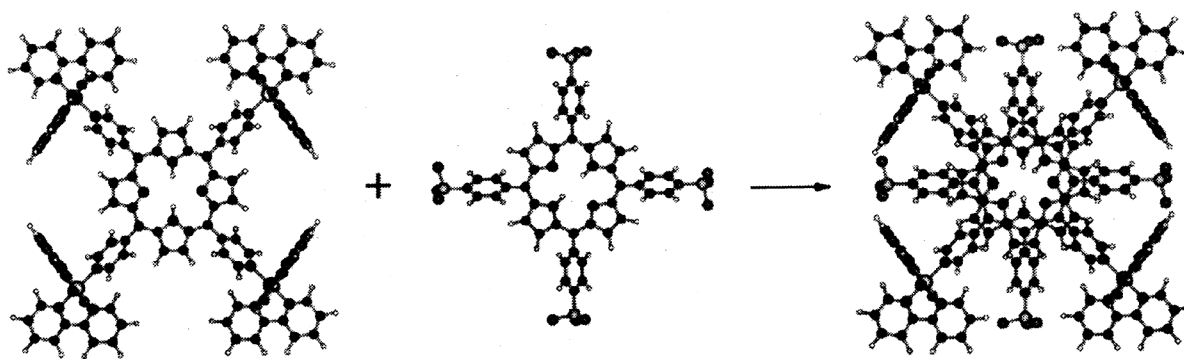
Figure 10. Molecular simulation of the electrostatic assembly of $[TRPyP]^{4+}/[TPPS]^{4-}$ species.

electrochemical wave around 0.36 V, when the electrode surface is coated with the supramolecular species. As a matter of fact, the $[M(TRPyP)]X_4$ films are not conducting within the potential interval between two successive redox waves, e.g. from −0.5 to 0.6 V in aqueous solution. However, at the onset of the $Ru^{III/II}$ redox wave (e.g. ~0.7 V), there is a sharp increase of the current (Figure 9). At this potential, the $Ru^{III/II}$ redox pair opens the electrochemical gate for the discharge of the ferrocyanide ions, by means of an electron-hopping mechanism.

The lack of the characteristic ferrocyanide wave at 0.36 V, is a good indicator of the absence of holes, cracks and other types of imperfections, which otherwise would allow the diffusion of electroactive species and their direct electron exchange with the electrode surface. Similar results have also been reported using $[Ru^{II}(edta)(H_2O)]^{2-}$, ascorbic acid and NADH as substrates, indicating that the existing channels for electrolyte migration in the films should be relatively narrow to prevent the diffusion of molecular species[42,81,84,87,88].

Electrostatic assembly

Another strategy, involving electrostatic assembly, has been developed to build-up more stable films, preserving the conduction and electrochemical properties. Such alternative is based on the strong interaction between the tetracationic species $[M(TRPyP)]^{4+}$ and the tetraanionic $[M'(TPPS)]^{4-}$ molecules, by means of electrostatic and π-interactions. The ion–pairing process is directed by molecular recognition because the structural and electric charge of those species is complementary, as one can see in Figure 10. In fact, a face-to-face dimer is initially formed when they are mixed together in dilute methanol solution, as confirmed by the sharp and blue-shifted Soret band indicative of a strong exciton coupling between parallel transition dipole moments. In more concentrated solutions, the aggregation of the ion-pairs leads to deposition of an insoluble material. Interestingly, this material can be assembled, in a controlled way, layer-by-

layer, generating ultrathin films on substrates such as silicon wafers and ITO plates[82,83,86,88]. A similar approach has been successfully employed for generating electrostatically self-assembled polymeric films, as electrode modifiers, displaying outstanding catalytic activity[89–93].

The electrochemical behaviour of the electrostatic assembled films has been observed to be very similar to that of pure M(TRPyP) modified electrodes, exhibiting a pair of sine-shaped waves at $E_{pc} = 0.90$ and $E_{pa} = 0.98$ V for the $Ru^{III/II}$ redox couple. The surface concentration per bilayer has been estimated as 7.5×10^{-11} mol cm^{-2} and the charge diffusion through the film is rather fast ($D_{CT} = 3 \times 10^{-11}$ cm^2 s^{-1})[47,90,95]. Four conduction mechanisms are possible: (i) electron hopping through the peripheral ruthenium complexes, (ii) electron hopping through the stacked metalloporphyrin rings, (iii) electronic conduction through the porphyrin π-stacks and (iv) hole-transfer from the electrode to a ruthenium complex and propagation through the porphyrin π-stacks. The impedance spectra have shown that the conductivity increases as the potential approaches the $E_{1/2}$ of the Ru(III/II) process, as expected for a redox conduction mechanism involving the peripheral ruthenium complexes[94].

Electropolymerized films of tetraruthenated porphyrins

Eletropolymerization is specially interesting for providing a better control of the local and amount of the deposited film[47,96–114]. It can be carried out by introducing electropolymerizable groups, such as 5-chlorophenanthroline (5-ClPhen). A reductive dimerization of 5-ClPhen has already been reported by Fussa-Rydel et al[115]. and provides an interesting strategy for the electropolymerization of meso-tetra(pyridyl)porphyrins attached to four [Ru(5-ClPhen)$_2$Cl]$^+$ groups. Two methods have been applied for generating such species, called ETRPyP (electropolymerizable tetraruthenated porphyrins)[47]: a) the direct electropolymerization from a dimethylformamide solu-

tion and b) the electropolymerization of a preformed film by dip coating, in acetonitrile solution, as shown in Figure 11.

The voltammograms of ETRPyP exhibit reversible waves at $E_{1/2}$ = 1.00 and –0.65 V in DMF solution, which have been assigned to the Ru(III/II) redox pair and to the monoelectronic reduction of the porphyrin ring to the π-radical anion respectively, and a shoulder at E_{pc} = –1.04 V ascribed to the formation of the respective porphyrin dianion (Figure 11). The monoelectronic reduction of a 5-Clphen ligand of each peripheral ruthenium complexes occurs at E_{pc} = –1.11 V. Its anodic wave is broad, more intense and is shifted to positive potentials because of the overlap with the anodic wave corresponding to the reoxidation of the porphyrin dianion. The reduction of 5-ClPhen induces the elimination of chloride and formation of phenanthroline radicals[115] that react promptly with each other forming a C–C bond (Figure 11). The H_2(ETRPyP) species has two of such ligand for each of the four peripheral ruthenium complexes, in a suitable arrangement to generate a polymeric film. Typical voltammograms in DMF (–1.3 to 1.2 V range) using platinum disk electrodes are shown in Figure 11. The stepwise increase of the Ru(III/II) wave along the successive scans results from electropolymerization process[97,101,104,106,108]. However, this procedure leads to poor quality films, due to the looseness of the presumably low molecular weight polymeric chain.

A better alternative procedure is to carry out electropolymerization directly on the films previously formed by dip-coating[3,42,45,47,81,82,84,86,95]. The high concentration of the monomer on the electrode surface and the presence of suitably pre-oriented molecules improve the electropolymerization, requiring only one or two scans in the 0.0 V
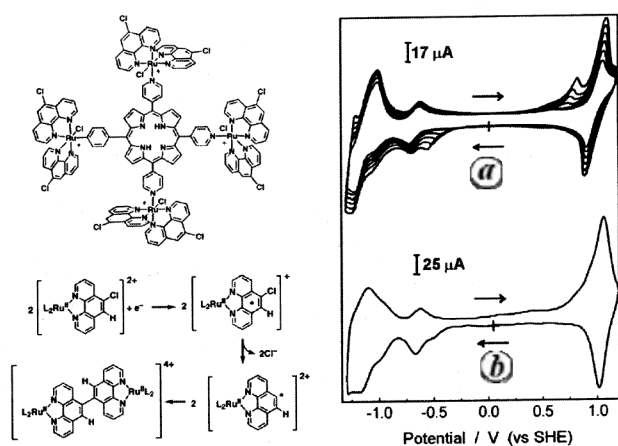

Figure 11. (Left) Structural representation of ETRPyP and the electropolymerization reaction; (Right) *a*, Successive cyclic voltammograms of 5.2×10^{-4} ETRPyP in 0.2 M TEAClO$_4$ DMF solution, scan rate = 100 mV/s, Pt disk electrode. *b*, Cyclic voltammogram of a Pt electrode modified with a polymeric ETRPyP film obtained by electropolymerization[47] of a dip-coated film, in 0.2 M TEAClO$_4$ acetonitrile solution, scan rate = 100 mV/s.

to –1.3 V range for completion, yielding a more compact and reticulated structure. A typical bell-shaped voltammogram has been obtained for a platinum electrode modified with a thin polymeric H_2(ETRPyP) film in acetonitrile electrolyte solution, as shown in Figure 11. The ITO electrodes modified by dip-coating have also been examined by AFM microscopy, before and after the electropolymerization process. The AFM images (Figure 12) show that the dip-coated samples consist of small aggregates more or less uniformly distributed onto the ITO surface, while the electropolymerized films exhibit larger features, reflecting the occurrence of structural changes and molecular reorganization.

The conduction properties of the electropolymerized supermolecular porphyrin films (0.65–1.25 V range) have also been probed by impedance spectroscopy. The Nyquist plots of the data obtained at different equilibrium potentials for a surface coverage of $\Gamma = 4 \times 10^{-9}$ mol cm^{-2} show that the charge-transfer resistance decreases sharply as the applied potential approaches the Ru(III/II) redox potential[13]. When the potential is increased further, the observed profile of conductance vs potential plot becomes very similar to the voltammetric profile, confirming a redox mechanism of conduction[89,95,116–118].
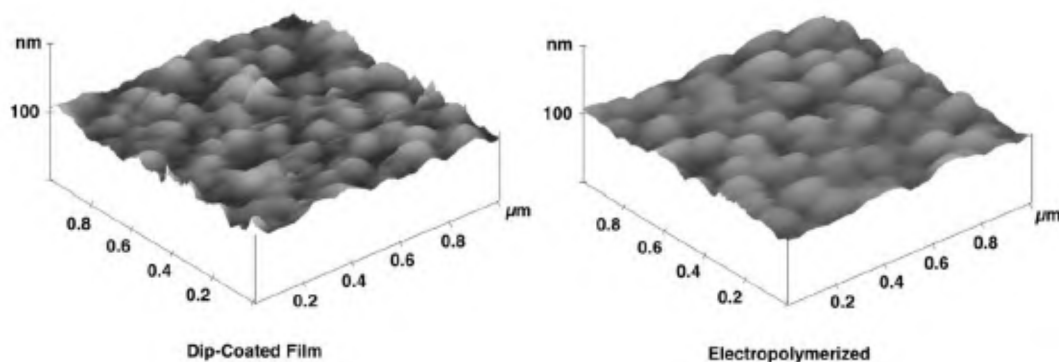
Supramolecular devices

Molecular machines and devices represent an innovation front in nanotechnology and are being pursued for energy conversion, sensors, displays and as nanosize version of the microscale components of MEMS and microelectronics[4,21,119–139]. As a matter of fact, a molecule can efficiently capture light or electrons and respond to electric or magnetic impulses, thus being able to process information. Specialized molecules can conduct electron (molecular wires), or pump electrons/photons (photonic pumps). Molecules can also be effective probes for molecular recognition. Combining such many abilities and properties, molecules can be designed to communicate with each other, signalizing this by means of color changes, emission of light and/or sound, release or uptake of protons and ions, etc. They can also be interfaced to a metal wire or fiber optics, transducing their response into measurable electrical or optical signals.

In general, a functional device is based on electrical and optical elements. In a simplified way it can be pictured by two conducting windows or electrodes as shown in Figure 13; one of them being coated with a thin film of the active molecular material. The electric contact between the electrodes is usually made with a suitable liquid or polymeric electrolyte containing a charge-transport mediator. This description applies relatively well for a number of devices, such as the LCDs (liquid crystal displays), OLEDs (organic light emitting devices), DSC (dye solar cells), smart electrochromic windows, amperometric sensors and logic gates.

Figure 12. Morphology of a dip-coated film before and after electropolymerization (2 scans) in acetonitrile solution, in the –1.3 to 1.2 V range.

Figure 13. Pictorial representation of a molecular device activated by photons or electrons, showing the conducting windows/electrodes, the semiconducting and/or functional molecular film and the mediator/electrolyte.

In this scheme, additional layers of semiconducting materiais, such as TiO_2, can also be employed, in combination with the molecular materials. The molecular interfaces play a major role in such devices, making contact with the active films and providing efficient directional access and transport of electrons and photons. For this reason, the nature and quality of the molecular films is a critical point. Such films can be prepared by several methods, e.g. thermoevaporation, dip-coating, spin-coating, drop-casting and Languir–Blodgett. Thermoevaporated supramolecular calixarene films have been successfully empolyed in OLEDs, displaying a tunable electroluminescent emission between 470 and 510 nm by changing the applied voltage bias from 4.3 to 5.4 V[140]. Another strategy for generating molecular films is based on electropolymerization of suitable oligomeric species[101], as well as on the layer-by-layer deposition of opposite electrostatically charged species (electrostatic assembly) as described in the previous section[85,141].

Amperometric sensors with supramolecular interfaces

Sensors can be viewed as special interfaces for communicating with the molecular world, since they involve some kind of transduction process for expressing the interaction/reaction of the molecular species with the sensing elements. For instance, the impedance changes of conducting polymers such as polypyrrol, polythiophene and polyaniline when in contact with different types of analytes, can be used to sense the quality and origin of wines and coffee[142–151]. However, in this particular case, the sensors rely on non-specific interactions of multiple compounds with the active materials, thus giving an average response.

Specially engineered thin films can provide selective molecular interfaces for many substrates but the requirements and characteristics will depend on the measurement techniques employed. A very useful one is the amperometric technique. In this case, the detection method is based on the measurement of faradaic currents, produced by the oxidation/reduction of a given analyte at the electrode surface. Suitable materials for amperometric sensors should exhibit (a) electron conducting (redox or electronic) and electrocatalytic sites, (b) size controlled pores through which the cations and/or anions from the electrolyte can diffuse rapidly, (c) good chemical and mechanical stability, (d) selective/specific response to substrates, and (e) resistance to surface poisoning. These requirements are important for analytical applications, but other aspects can also be relevant. In fact, the sensibility will depend on the electron transfer rates and diffusion of electrons/ions through the molecular material, as well as on electrocatalysis efficiency.

The M(TRPyP) and M(TCPyP) films provide conduction gates represented $Ru^{III/II}$ sites at 0.92 V, or by the metalloporphyrin center, which can be tuned by the applied potentials as they approach the corresponding redox potentials. The last one can be localized at the transition metal center (Co(III/II/I), Mn(III/II) and Fe(III/II)) or at the porphyrin π-ring system. The activation of the redox centers is susceptible to synergistic and induced elec-

tronic effects[45,51]. In some cases, a reduced metallopor-phyrin center, probably with M^IP character is responsible for the electrocatalytic activity, as observed in M(3-TRPyP), where M = Ni, Co and Mn[152-154]. On the other hand, the oxidation of substrates such as ascorbic acid, NADH, dopamine, acetaminophen, phenol, nitrite and sulphite occurs by an outer-sphere mechanism involving the peripheral ruthenium complexes[16, 86-89, 95,155].

An interesting application of such supramolecular films is in the detection of sulfur dioxide and its source compounds, such as the sulfite salts, which are added to foods and beverages in order to inhibit bacterial growth, to prevent oxidation and inhibit discoloration, thus improving the final appearance of the products[12,81,87,152,156-158]. Only SO_2 exhibits antiseptic properties[159-166] but, at high levels it produces an unpleasant aroma and taste, besides being hazardous to human health. The analysis of free and total sulfur dioxide in wine has been carried out using a diffusion cell on line with the FIA (flow injection analysis) amperometric detector based on the M(TRPyP) and M(TCPyP) films (Figure 14). A gas diffusion cell is necessary for the transference of the gaseous compounds from the donor stream to the acceptor one, through a semipermeable membrane.

As a matter of fact, the CoTRPyP films provide a considerable enhancement of the sulphite response and decrease of the overpotential, shifting the oxidation wave to the onset of the $Ru^{II/III}$ redox wave. A similar behaviour has been observed for the electrostatically assembled CoTRPyP/ZnTPPS films[81,87]. The consistency of the FIA method using modified electrodes is quite good, and the method can be scaled up to a large number of samples.

Nitrite ion is another interesting analytical substrate because of its prevalence in industrialized meats as pre

serving agent and appearance builder, also. But, when ingested it can react with hemoglobin oxidizing it to meta-hemoglobin, and with amines converting them to nitrosamines, which are well-known carcinogenic substances[167-170]. The environmental impact caused by high concentrations of nitrite and nitrate ions from the inadequate use of fertilizers, and the contamination of water sources for human consumption are also big concerns[171,172]. Interesting results have been obtained using glassy carbon electrodes modified with layer-by-layer electrostatic assembled films of Ni(TRPyP)/CuTSPc and Co(TRPyP)/CuTSPc, in the presence NO_2^- and SO_3^{2-} species. Both modified electrodes exhibit enhanced catalytic current at the onset of the $Ru^{III/II}$ wave (0.9 V), including significant decrease of the overpotentials for the sulphite ions. Because of the distinct electrochemical signals, the two species can be simultaneously analysed in a mixture.

Electropolymerization makes the $[H_2(4TPyP)\{Ru(5-Clphen)_2Cl\}_4]$, or $H_2(ETRPyP)$ films rather interesting for application in amperometric analysis, specially for the preparation of microelectrode arrays. Analogously to the M(TRPyP) films, a catalytic current has been observed for the electropolymerized films in the oxidation of nitrite to nitrate, mediated by the Ru(III) species[47,81,87,89,95,152,156,157,173]. The kinetics of oxidation of nitrite to nitrate have been studied by RDE voltammetry, from 200 to 8000 rotations per minute, and in the 1×10^{-5} to 1×10^{-3} M concentration range. A typical sigmoidal
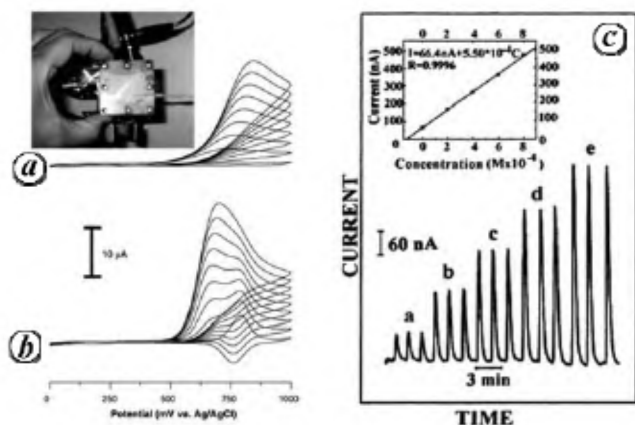
Figure 14. Cyclic voltammograms of SO_3^{2-} ions using (*a*) bare glassy carbon electrode and (*b*) the CoTRP/ZnTPPS coated electrode, (*c*) and its corresponding FIA response for free SO_2 concentrations in white wine (sample a, Forestier); the FIA cell is shown above.
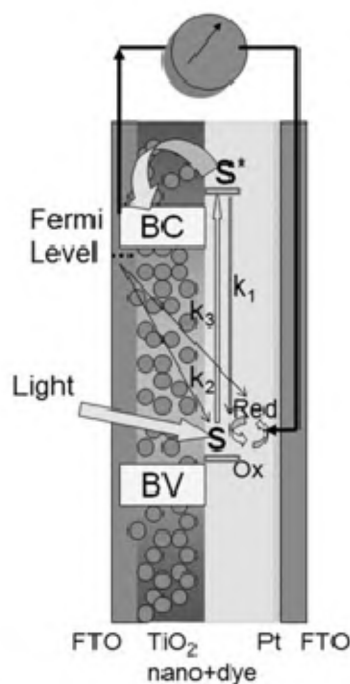


Figure 15. Representation of a dye solar cell (DSC) incorporating the sensitizer (S) adsorbed at the nanocrystalline semiconductor interface (TiO_2).

shaped profile has been observed, characteristic of a rapid reaction. The corresponding rate constant has been obtained from the linear coefficients of the Koutech–Levich plots as $k_f = 3.7 \times 10^4 \, M^{-1} \, s^{-1}$ This value is one order of magnitude higher than that previously obtained[13,47] for the Co(TRPyP)/Zn(TPPS) electrostatic assembled bilayer films.

Another important application of the supramolecular porphyrin films is in the determination of drugs such as acetaminophen in pharmaceutical formulations. This work has been recently performed[88], by means of batch injection analysis (BIA) based on amperometric detection with glassy carbon electrodes modified with [Co(4-TRPyP)](CF$_3$SO$_3$)$_5$ films. This sensor exhibits sharp current response, rapid washout and excellent reproducibility for BIA-amperometric quantification of acetaminophen. The proposed method permits the direct and selective quantification of acetaminophen in many pharmaceutical products, avoiding cumbersome processes as previous separations, solvent extraction or sample filtration.

Supramolecular photoelectrochemical devices

Photoeletrochemical cells employ a conducting glass electrode coated with a thin film of a semiconducting material placed in contact with a suitable redox couple, e.g. I_3^-/I^-, responsible for mediating the electron transfer to a second electrode, as illustrated in Figure 16. The most commonly used semiconductors are based on ZnO, WO$_3$, SnO$_2$ and TiO$_2$, which are typically wide band gap materials[174].
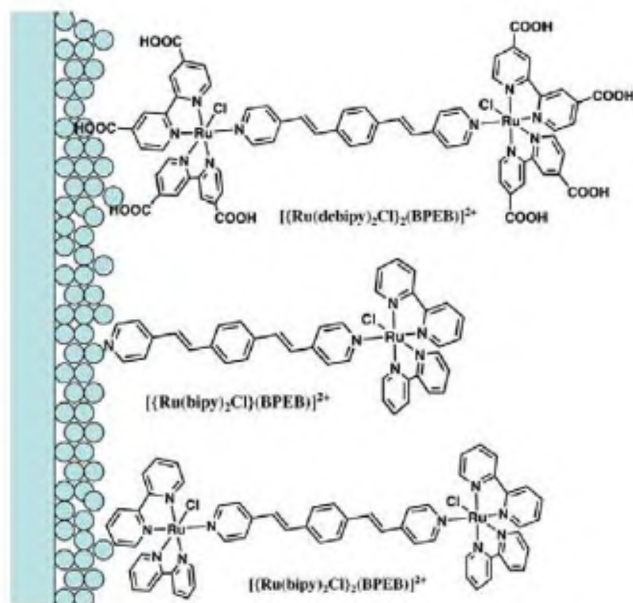
Figure 16. Ruthenium bipyridine dyes incorporating the conjugate BPEB ligand.

Light absorbed by the semiconducting material promotes electrons to the conduction band (CB), generating holes at the valence band (VB). The redox mediator supplies the electrons to the valence band, undergoing oxidation, and is regenerated at the cathode, closing the electric circuit. The amount of electrons produced by absorbed photon of a given wavelength is expressed by the IPCE value. In order to evaluate the overall efficiency (η) of the solar cell, it is necessary to obtain a current vs potential (I–V) curve, and calculate the filling factor (FF) comprising the maximum rectangular area which can be inserted in this plot, corresponding to $P_{max} = I_{max} \cdot V_{max}$. The cell efficiency is given by $\eta(\%) = P_{max}/(irradiance \, area)$.

Conventional semiconductor photoelectrochemical cells usually exhibit a rather small efficiency, in part because the optical absorption of the wide band gap semiconducting films requires UV light excitation, thus making poor use of the available visible near-infrared radiation of the sunlight. In order to overcome this limitation, the use of dye-sensitizers in association with wide band gap semiconductors has been pursued with great interest, since 1970 decade.

The ideal dye should absorb a broad spectrum of light from the near UV to the NIR region encompassed by the distribution of the spectral radiation of the sun (also referred as AM 1.5). Its excited state should be located above the conduction band (i.e. at more negative potentials) in order to allow efficient photoinjection of electrons to the TiO$_2$ layer. In the case of a good TiO$_2$/dye interface this process is usually very fast (10^{-12} s), competing favourably with the radiative decay processes (k$_1$) or any possible photochemical reaction. The ground state should exhibit a redox potential more positive than that of the redox couple mediator (e.g. $E°(I_3^-/I^-) = 0.4$ V), in order to undergo a rapid regeneration (< 1 μs), and should also be electrochemically stable, in order to allow a very large number of cycles without undergoing decomposition reactions. A fast electron transfer kinetics involving the mediator/electrode interface is also important. Surface activation with platinum catalytic particles can strongly improve the electrode kinetics. Recombination processes (k$_2$ and k$_3$) involving the semiconductor Fermi levels and the oxidized dye (D$^+$) or mediator (I$_3^-$) can decrease the photocurrent yield, and should be minimized by improving the conductivity and the interface design. The open circuit voltage (V$_{oc}$) is established by the Fermi levels of the semiconductor layer and the redox potentials of the mediator.

The most extensively investigated dyes were derived from ruthenium(II) polypyridine complexes, and the standard dye currently used in DSC experiments is the [Ru(dcbipy)$_2$(NCS)$_2$] complex, also referred as N3. The use of dyes has allowed to extend the photoinjection response to the visible region; however, in spite of this, the efficiency of such dye-sensitized solar cells (DSC) in

terms of the irradiated area remained quite small (IPCE < 0.15%) until 1991. In this year, a great improvement has been achieved by Gratzel and O'Reagan[175] by using nanocrystalline TiO_2 films exhibiting high surface-to-area ratio, in addition to good light transparency, charge-separating properties and electronic conductivity (Figure 15). The IPCE in this case, increased by three orders of magnitude in relation to the previous dye cells, jumping from 0.12% to 90%, for an active area of 1.3 cm^2.

The work of Grätzel and O'Reagan has stimulated the use of the nanotechnological approach in DSC, and culminated in a recent overview on the state-of-art of the subject[176]. Their activities from 2002 until 2004, were focused on demonstrating new strategies for DSC concepts, including co-sensitization, cell materials and fabrication protocols for TiO_2 pursuing an increase of efficiency to >12% under Standard Test Conditions (AM1.5, 1000 W/m^2), and a long term stability[176–192]. Cost analyses have been made to demonstrate the potential of DSC as a low cost thin film photovoltaic technology, exhibiting a maximum efficient under full sunlight of 11% for a cell with an active area < 0.2 cm^2, and 10% for an active area of 1.3 cm^2.

TiO_2 surface modification has been attempted by using very thin tunneling barrier layers and co-sensitization strategies employing dye multilayers. The use of other metal oxides such as Nb_2O_5, ZnO and SnO_2 replacing TiO_2 has also been investigated[176,193]; however, to date, no one has been able to improve on the efficiencies obtained using TiO_2.

The electrolyte used in high-efficiency cells consist of alkylimidazolium iodides or tetra-alkyl ammonium iodides, lithium iodide/I_2 in solvents such as acetonitrile, propionitrile or mixtures of acetonitrile and valeronitrile. In addition to *tert*-butylpyridine and benzimidazole, new surface additives based on carboxylic and phosphonic organic acids have been employed to facilitate the self-assembly of the dye molecules at the TiO_2 electrode surface, rendering it more impermeable, and reducing the dark current of the cell.

Innovative strategies, such as the use of supramolecular dyes[28–30,49,50,178,194–196] can reduce the dispersive kinetics, improving the device efficiencies. Haque et al.[197] have proposed the dye chromophore modification by the covalent attachment of secondary electron donors. The electron-transfer cascades in such supramolecular structure can retard the charge-recombination dynamics by increasing the physical separation between the dye-cation moiety and the TiO_2 surface. By means of transient absorption spectroscopy, they have shown that charge-recombination dynamics in the [$Ru^{II}(dcbpy)_2(RBpy)$] dyes containing aryl-amine (R) based electron donor groups decrease linearly by 5 orders of magnitude, as a function of the spatial separation from the TiO_2 surface, of the dye cation generated after the photoinjection process.

Another interesting case has been reported for ruthenium(II) bipyridine and dicarboxybipyridine (dcbpy) complexes containing the *trans*-1,4-bis[2-(4-pyridyl)ethenyl]-benzene (BPEB) ligand (Figure 16). The BPEB ligand is a typically conjugated bridging ligand which can allow intramolecular photoinduced electron-transfer or energy-transfer processes between the two ruthenium moieties.

The absorption spectrum of the BPEB bridged species, [{$Ru(dcbpy)_2Cl$}$_2$(μ-BPEB)]$^{n-}$ in aqueous solution is shown in Figure 17, together with the incident photon-to-current conversion efficiency (IPCE) curves as function of wavelength.

The IPCE curve of such species exhibits a broad band from 400 to 600 nm with a maximum centerd at 520 nm. The observed IPCE values are comparable to those exhibited by the N3 reference complex[198–200]. The bathocromic shift of the absorption bands (~ 40 nm) of the [{$Ru^{II}(dcbpy)_2Cl$}$_2$(BPEB)]$^{6-}$ dye anchored on TiO_2 reflects the binding of the carboxylate groups to the surface. The binuclear species can make use of one or two dcbpy ligands in the anchoring process to TiO_2, generating a linear or a flat arrangement at the surface. As illustrated in Figure 16, the linear arrangement leads to a less symmetric configuration in which the TiO_2 binding side has a lower energy. This facilitates a vectorial electron transfer from the other extremity, resulting in a more effective charge-separation, and a higher IPCE value.

A comparison of [{$Ru(dcbpy)_2Cl$}$_2$(BPEB)]$^{6-}$ with the related [{$Ru(bpy)_2Cl$}$_2$(BPEB)]$^{2+}$ and [$Ru(bpy)_2Cl$-(BPEB)]$^+$ species containing a non-carboxylate bpy ligand, and pristine TiO_2, can also be seen in Figure 17. Such species exhibit much lower IPCE, as a consequence of the lack of effective anchoring groups. Surprisingly, the mononuclear [$Ru(bpy)_2Cl(BPEB)$]$^+$ species presents
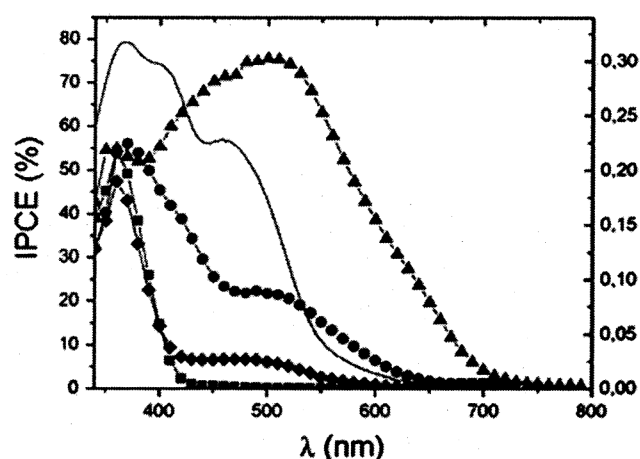
Figure 17. Incident photon-to-current conversion efficiency (IPCE) curves as a function of wavelength for the sensitizers: (–▲–) [{$Ru^{II}(dcbpy)_2Cl$}$_2$(BPEB)]$^{6-}$(1); (–◆–) [{$Ru(bpy)_2Cl$}$_2$(BPEB)]$^{2+}$(2) and (–●–)[$Ru(bpy)_2Cl(BPEB)$]$^+$(3), and for bare TiO_2(–■–). The absorption spectrum of the binuclear species [{$Ru^{II}(dcbpy)_2Cl$}$_2$(BPEB)]$^{6-}$ in aqueous solution is also shown in full line.

IPCE values reaching 50 and 20% around 400 and 500 nm, respectively, while the IPCE values for the binuclear [{Ru(bpy)$_2$Cl}$_2$(BPEB)]$^{2+}$ are almost negligible. These results show the dramatic importance of the anchoring groups. Even in the case of the mononuclear species, the comparison with the corresponding binuclear species reveals the important role of the free pyridyl group on the BPEB ligand, in promoting the chromophore binding to the TiO$_2$ surface.

It is interesting to note that zinc tetrapyridylporphyrins (TPyP) coordinated to four [Ru(bipy)$_2$Cl]$^+$ and [Ru (phen)$_2$Cl]$^+$ complexes, i.e. Zn(TRPyP) and Zn (TRpPyP)[16,17] adsorb onto TiO$_2$ even without the carboxylate anchoring groups, producing photoelectrochemically active red-brown films[46,49,55,201]. Typical photoaction spectra (IPCE curve vs λ) of the photoelectrochemical devices assembled with TiO$_2$/TRuphen-ZnTPyP films exhibit strong photoaction response at 350 nm from the direct excitation of the TiO$_2$, but the IPCE curves resemble the absorption spectrum of the supramolecular dye, displaying the characteristic Soret, MLCT, and two Q bands at 440–450, 480–530, 575 and 620 nm respectively[202–204]. The similarity between the absorption and photoaction spectra indicates that the porphyrin and peripheral ruthenium complexes are contributing to the photocurrent. Analogously to the Zn(4-TRpPyP) species, the IPCE values for Zn(4-TRTPyP) reach 13% at the maximum absorption (Soret band) of the supramolecular dye, much higher than those observed for bare TiO$_2$ and free base TRpPyP and TRPyP (both without Zn). The porphyrin bands are red-shifted with respect to the species in solution, indicating that the supramolecular species are interacting with the TiO$_2$ surface via porphyrin core. In contrast, the free base supramolecules, TRPyP and TRpPyP, practically do not adsorb onto TiO$_2$. As a consequence, no photocurrent has been detected. This result is clear evidence that the attachment of supramolecular metalloporphyrins involve the central Zn(II) ion and the hydroxyl groups of the TiO$_2$ surface, as previously reported in the literature for another zinc porphyrin system[13,49,50,82,205].

Photoelectrochromic devices

Electrochromism represents the reversible color changes exhibited by a material or system upon inducing oxidation/reduction processes by means of an applied potential. It has been successfully employed in automotive rearview mirrors, and is expected to evolve considerably in the next years. There are at least four types of electrochromic devices[206]. One is based on the color change of a layer of a transition metal oxide, such as WO$_3$, NiO, MoO$_3$, IrO$_2$ and Co$_2$O$_3$, deposited on a transparent conducting electrode. Such systems seem to be stable enough to allow their incorporation in architectural windows; however, they suffer from the drawback of slowness or insufficient color change. Another type of device employs Prussian blue complexes as electrochromic materials. The third type is based on the electrochromism of conducting organic polymers, such as polyaniline, polypyrrole and polythiophene. The fourth type of electrochromic devices exploits the use of wide band-gap nanocrystalline semiconductors functionalized with charge-transfer compounds[207–210].

The attachment of a redox chromophore to a semiconducting nanoparticle surface, allows to increase the coloration of the films due to a high concentration of chromophores and to achieve fast switching times. Several redox molecules containing a surface anchoring group have already been investigated, including the well-established viologens[198,211–213], and several metal complexes with different ligands[214–216]. The basic arrangement is similar to that for a typical photoelectrochemical dye cell (Figure 15), however, in this case the electrons are injected from the conducting substrate into the conduction band of the semiconductor and from there, to the adsorbed electroactive dye. If the redox potential of the dye lies below the conduction band, the electrochromic process can be reversed by the application of a positive potential to the conducting substrate.

The *trans*-1,4-*bis*[2-(4-pyridyl)ethenyl]benzene (BPEB) complexes exhibit an interesting electrochromic behavior, resembling that of viologen compounds. The ligand first reduction generates the radical (BPEB$^{1-/0}$), giving rise to two strong near infrared bands centered at 718 and 781 nm, turning the electrode blue. These bands correspond to $\pi \rightarrow \pi^*$ transitions in the radical cation. In contrast, the second reduction gives rise to BPEB$^{2-/1-}$ species, which are almost colorless.

The electrochromic behavior of BPEB has also been explored in the TiO$_2$/[{Ru^{II}(dcbpy)$_2$Cl}$_2$(BPEB)]}$^{6-}$ system. The complex molecules chemisorbed on the nanostructured TiO$_2$ electrode undergo a single electron reduction in the potential range from -0.7 V to -1.0 V vs SHE, corresponding to the formation of the radical anion in the BPEB ligand, coloring the electrode blue. This reduction process is accompanied by a change of 42% in the film transmittance, from almost transparent to deep blue. The electrode color is completely recovered after each oxidation-reduction process. The coloration efficiency CE(λ) at 633 nm can be defined in terms of absorbance changes (ΔA) and charge involved (ΔQ), by CE(λ) = $\Delta A(\lambda)/\Delta Q$ = 109 cm^2 C^{-1}. This value is quite high if compared to TiO$_2$ itself (8 cm^2 C^{-1} at 633 nm) and to other electrochromic transition metal oxides, e.g. NiO$_x$ (40 cm^2 C^{-1}), CoO$_x$ (50 cm^2 C^{-1}), being similar to WO$_3$ (70–100 cm^2 C^{-1}).

Another interesting electrochromic system is based on the TiO$_2$/[Ru$_3$O(CH$_3$COO)$_6$(py)$_2$(BPEB)]$^+$ system. The electronic spectrum of this complex consists of the BPEB intra-ligand (IL) $\pi - \pi^*$ transitions centered at 370 nm, the cluster-to-ligand charge transfer (CLCT) around

400 nm and the characteristic internal transitions (IC) of the [Ru$_3$O] core between 600 and 800 nm. It should be noted that the [Ru$_3$O(OOCCH$_3$)$_6$(py)$_2$(BPEB)]$^+$ cluster exhibits a free pyridine group, facilitating its adsorption to mesoporous TiO$_2$ films. Its reversible electrochemical response is preserved when anchored on the TiO$_2$ surface.

In the case of the mesoporous TiO$_2$ films modified with the triruthenium cluster, the electrochromic behavior observed from −0.2 to 0.5 V, in the presence of ferrocene (Fc) ions as mediator, is related to the redox process of the [Ru$_3$O] core, as shown in Figure 18. Analogously to the behavior in solution, a reversible electrochromic process is observed, changing the colors from yellowish-green to violet. The spectral changes between 0.5 and −1.0 V are related to the first reduction process of the Ru$_3$O core in the {[Ru$_3$O(OOCCH$_3$)$_6$(py)$_2$(BPEB)]}PF$_6$ complex, i.e. Ru$_3$O$^{+/0}$, showing a decrease of the intracluster band at 680 nm and the rise of the cluster-to-ligand charge transfer and intracluster bands at 522 and 918 nm respectively.

The chronoamperometric behavior recorded, successively, after 5 s intervals between −1.0 and +0.5 V, can be seen in Figure 18 b. At −1.0 V the sharp initial electrochemical response is associated with the cluster reduction

Figure 18. (*a*) Spectroelectrochemistry and (*b*) chronoamperometry of the TiO$_2$/[Ru$_3$O(CH$_3$COO)$_6$(py)$_2$(BPEB)]$^+$ electrochromic device between 0.5 and −1.0 V.
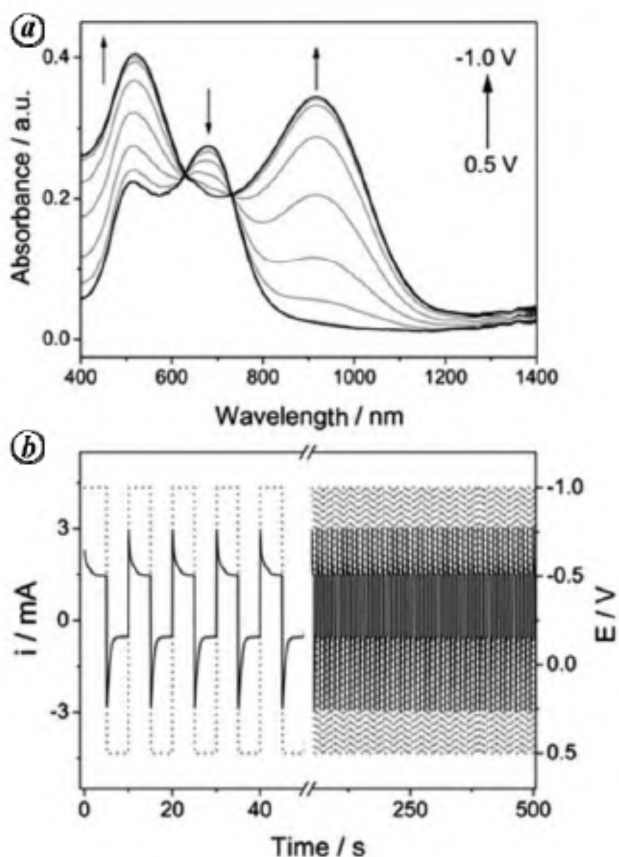
process onto the TiO$_2$ surface, leading to a drastic color change. This process is followed by a fast current decrease, up to a steady state condition (parasitic current). In the electrochromic device, this process is concomitant with the oxidation of the ferrocene (Fc) to ferrocenium ion (Fc$^+$) on the counter-electrode. This observation suggest that the steady-state currents arise from the continuous re-oxidation of the reduced cluster species, presumably by Fc$^+$ formed at the counter electrode.

The coloration time, which is the time to produce 75% change in the optical density, is smaller than 0.5 s. Completely reversible electrochemical and optical changes have been observed for many hundred cycles. The reported coloration efficiencies are 50 and 190 cm^2 C^{-1} at 692 and 920 nm respectively, which is quite high if compared with TiO$_2$ itself (8 cm^2 C^{-1} at 633 nm) and other electrochromic transition metal oxides[217–219].

Electrochemical and photoelectrochemical logic gates

Current information technology involves processing of input signals by means of the so-called logic gates[133, 220–226]. Data processing based on silicon circuitry requires the binary encoding of information contained in electrical signals; for each signal a threshold value and a logic convention are defined, according to the so-called Truth Tables describing the several logic gates: AND, OR, NOR, NAND, XOR, etc. For instance, a logic convention can relate to 0 for a signal value below the threshold, and to 1 for a value above the threshold. However, the binary logic is a rather general concept which can be applied to any type of signal, including chemical, optical and electrochemical ones.

Molecular systems can be employed for the implementation of logic functions, addressed by external stimuli input (for example, photons, electrons, chemical entities) in order to generate one or more answer signals as outputs[227–229] (for example, chemical reactions, light emission, changes in electronic and electrochemical properties). Recently, several examples of molecules have been reported emulating the functions of memories[230–234], switches[229,231,235–237], wires[238–241], rectifiers[242] and logic gates[6,127,221,222,224–226,228,243,244]. A logic gate can enable information processing and computation at the molecular level. Examples of molecular logic gates have already been described[4] but are based on reactions in solution. Zauner and Conrad[245] have proposed an enzyme based XOR gate, where the signals were generated by monitoring the malate dehydrogenase absorbance as a function of Ca^{2+} and Mg^{2+} co-factors (inputs). Stoddart and co-workers[231] have demonstrated the capability of rotaxane based molecular shuttles to promote logic functions and recently they described electronic devices operating in a molecular level[246]. Heinrich et al.[247] explored spon-

taneous molecular arrangements called 'molecular cascades' to construct logic gates. Alternative computation schemes have been proposed on electron confined systems, such as 'quantum dot cellular automata'[248] or 'magnetic dot cellular automata'[249–252]. Miyashita et al.[253] also described an AND logic gate based on optical properties of a polymer film. A remarkable series of all-photonic molecular logic gates has been recently reported by Moore and co-workers[254–256]. Another interesting fluorescent AND logic gate has been reported by Magri et al.[257] and Uchiyama et al.[258] involving 3 nm tetramethylammonium dodecyl sulphate (TMADS) micelles, containing a three-component molecular system.

The idea of using molecular films as interface is attractive because they provide intrinsic nanoelectrodes[259], allowing the miniaturization down to the molecular level. It has already been shown that the ultrathin supramolecular porphyrin films behave as excellent transducer elements, capable of converting chemical inputs into electrical signals. The heterogeneous electron-transfer at the film/solution interface and the photochemical reactions used as base of the molecular logic gates are rapid and the operation is relatively simple, requiring only small amounts of the molecular species solution (<100 μl per injection). In fact, the processes based on electron-transfer reactions can be faster than the mechanical work at molecular level[260,261]. However, on the other hand, it is necessary to overcome the difficulties associated with the transport of the molecular species (inputs) through the film/solution interface, for exploiting simultaneously their different properties, as genuine transducer elements, in order to generate controlled signal inputs and outputs
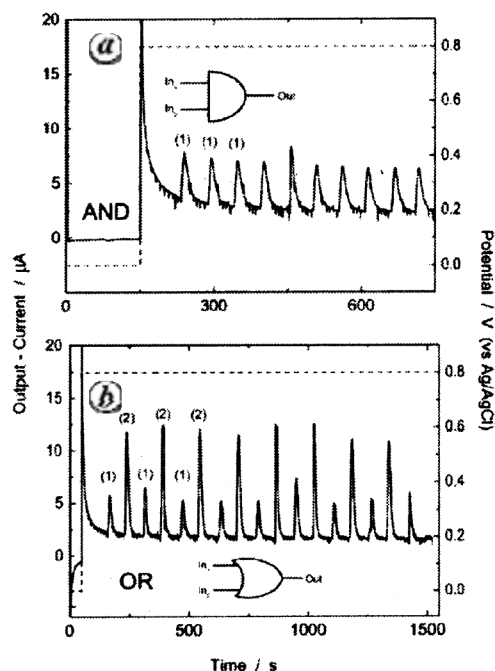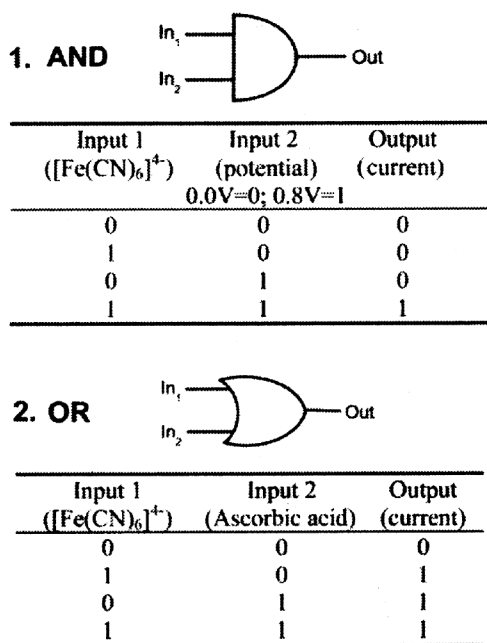
For this purpose, a flow injection analysis (FIA) cell using a tetraruthenated porphyrin film modified electrode has been designed for the realization of hybrid molecular logic gates. Such a device has the advantage of incorporating an amplifying function, resulting from its electrocatalytic and photoelectrochemical properties[126]. Reproducible analytical signals have been obtained in generating the FIA patterns after injecting consecutively a solution of ferrocyanide, keeping the potential of the modified electrode fixed at 0.0 V and then stepping to 0.8 V, as shown in Figure 19. Only when the potential is set to 0.8 V and the ferrocyanide solution is injected, a characteristic anodic peak is generated. Otherwise no current flows. A similar result is expected when ascorbic acid is used instead of ferrocyanide in the setup described above. However, one can use both of them as inputs keeping the potential constant at 0.8 V. In this case, an anodic peak is always observed when any or both of the solutions are injected (Figure 19 b). It should be noted that the current intensity obtained for the injection of solutions of ascorbic acid and ferrocyanide with the same concentration (1.0×10^{-4} M) generate peaks of roughly the double of the intensity for the first one because, respectively, two and one electrons are involved in the oxidation reactions.

By taking the electrochemical potential and the presence of ferrocyanide as inputs, one can set them in such a way that only when two affirmative inputs are simultaneously applied an affirmative response is generated as output (anodic peaks in Figure 19). Accordingly, the bit configurations are: input 1 is a chemical input and the '0' or '1' means absence or presence of $[Fe(CN)_6]^{4-}$, while input 2 is '0' or '1' for applied potential of 0.0 or 0.8 V. Considering these settings, the truth table shown in Figure 19 is obtained, which is equivalent to that of an AND gate.

The OR operation has two inputs and one output, just like the AND operation, but in this case only one affirmative input should be enough to generate an affirmative output. The OR operation can be obtained in a flow injection device by using two chemical inputs: ascorbic acid and ferrocyanide. They are set as '0' or '1' when $[Fe(CN)_6^{4-}]$ = [ascorbic ac.] = 0 or $[Fe(CN)_6^{4-}]$ = [ascorbic ac.] = 1×10^{-4} M, respectively, keeping the potential applied to the modified electrode fixed at 0.8 V. In this case, the injection of any of those two chemical species will generate an anodic current as response (Figure 19).

In addition to the amperometric response, one can also exploit the photoaction response observed when electrodes coated with polymetallated porphyrin films are irradiated with visible light in the presence of O_2, or another suitable as electron receptor agent. This characteristic is exhibited by pure M(TRPyP) films, as well as by the electrostatic assembled M(TRPyP)/M'(TPPS) ones[47,83,87,152,156,157] and the electropolymerized ETRPyP modified electrodes[13,47]. When the porphyrin material is irradiated, the lowest energy excited state is rapidly accessed. This species is a better reductant than the ground state species roughly by a factor corresponding to the excitation energy (E_{00}) and can transfer electrons to receptor agents, such as dioxygen molecules, in the electrolyte solution. The transferred electrons can be supplied by the electrode, if the potential is set more negative than the flat band potential, generating a cathodic photocurrent. In this way, light and the photoactivity of the supramolecular films[13] can be used in combination with their electrocatalytic properties to generate electric signals.

This photoaction-based logic gate can be implemented in a typical FIA cell, but using transparent electrodes. A cathodic photocurrent is generated when the ETRPyP modified electrode is irradiated in the presence of O_2 solution and the electrochemical potential is set more negative than 0.28 V[13], which corresponds to the flat band potential (E_{fb}). A sequence of photo-chronoamperometry signals can be registered employing an O_2 saturated solution and turning on and off the light source, while setting the potential at 0.0 or 0.8 V. Very reproducible cathodic plateaus are obtained when the incident light is turned on and the electrochemical potential fixed at 0.0 V, which is below the flat band potential. However, when the electrochemical potential is shifted to 0.8 V the photocurrent is completely suppressed. By using the electrochemical po-

1. AND

Input 1 ([Fe(CN)₆]⁴⁻)	Input 2 (potential) 0.0V=0; 0.8V=1	Output (current)
0	0	0
1	0	0
0	1	0
1	1	1

Table header in LaTeX: Input 1 $([\mathrm{Fe(CN)_6}]^{4-})$ / Input 2 (potential) 0.0V=0; 0.8V=1 / Output (current)

2. OR

Input 1 ([Fe(CN)₆]⁴⁻)	Input 2 (Ascorbic acid)	Output (current)
0	0	0
1	0	1
0	1	1
1	1	1

Figure 19. Truth tables for the logic gates using a FIA cell containing a TRPyP modified electrode, and FIA signals (*a*) for consecutive injections of 0.10 mM $[\mathrm{Fe(CN)_6}]^{4-}$ monitored at 0.8 V); and (*b*) for sequential injections of 0.10 mM $[\mathrm{Fe(CN)_6}]^{4-}$ and 0.10 mM ascorbic acid solutions. The dashed lines indicate the potential applied to the electrode.
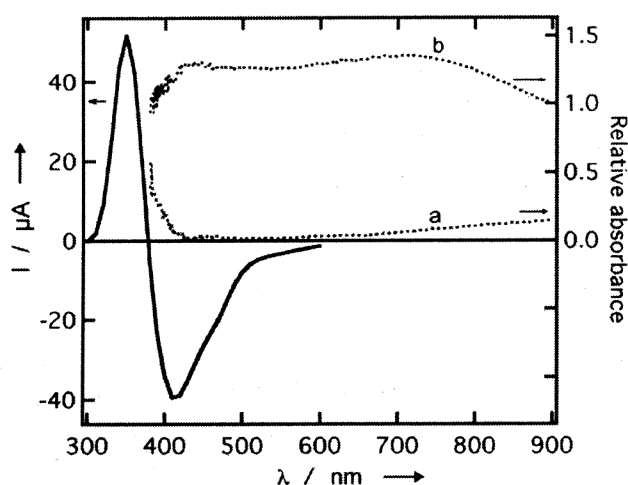
Figure 20. Photoaction response (solid line) of the device, and reflectance spectra (dotted lines) of a nanocrystalline $\mathrm{TiO_2}$ film on FTO (*a*) without and (*b*) with cluster sensitizer.

tential as input (0 V = input 0, and 0.8 V = input 1) and the photocurrent signal as output (0 and 1), a typical NOT gate is obtained. On the other hand, by using both, light (off = input 0, on = input 1) and the electrochemical potential (0 V = input 0, 0.8 V = input 1) as inputs A and B, respectively, the photocurrent output will be 1 only when A = 1 and B = 0, corresponding to an inhibited-AND gate, called INH.

An interesting molecular optoelectronic XOR logic gate operating exclusively with optical inputs and electric output, has been recently described, making the system easily addressable and compatible with the present electronics. This device is based on a $\mathrm{TiO_2}$ dye-sensitized Grätzel type cell[175,262], direct absorption of light by $\mathrm{TiO_2}$ (λ_{exc}<400 nm, Figure 20) produces a photoinduced charge separation, and if a dye can accept rather than inject electrons into the semiconductor layer when in the excited state, the photocurrent output direction can be modulated by the wavelength of the incident light, making possible the generation of a light-driven logic gate.

For this purpose, the molecular dye should be reductively quenched by the nanocrystalline semiconductor layer. Consequently, the ground state reduction potential should be more positive than about 0.0 V to satisfy this requirement using 2.5 eV photons (λ_{exc} ~500 nm) for excitation, since the energy of $\mathrm{TiO_2}$ valence band and the standard hydrogen electrode referenced to vacuum level are respectively 6.8 and 4.44 eV. Generally, the reduction potential of organic compounds and ruthenium polypyridine complexes such as N3 is more negative than –1.0 V, being typically photo-electron injectors. However, ruthenium acetate trinuclear clusters possess reduction potentials in a suitable range. In fact, the $[\mathrm{Ru_3O(Ac)_6(py)_2(pzCO_2H)}]\mathrm{PF_6}$ complex, (pzCO₂H = pyrazine carboxylic acid) exhibits such favourable aspects, and has been successfully used to demonstrate this hypothesis.
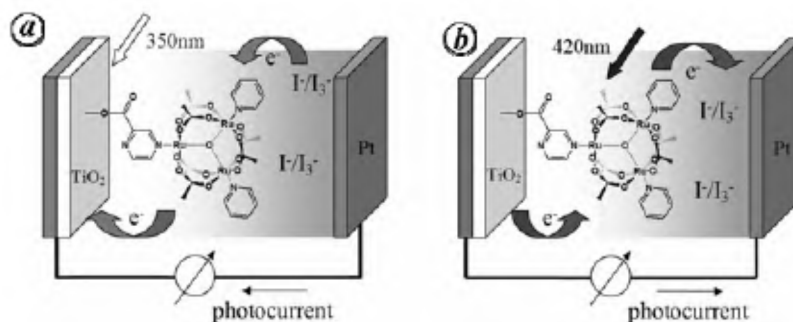
Figure 21. Scheme showing the mechanism of photocurrent generation in the $TiO_2/[Ru_3O(Ac)_6(py)_2(pzCO_2H)]PF_6$ photoelectrochemical cell.
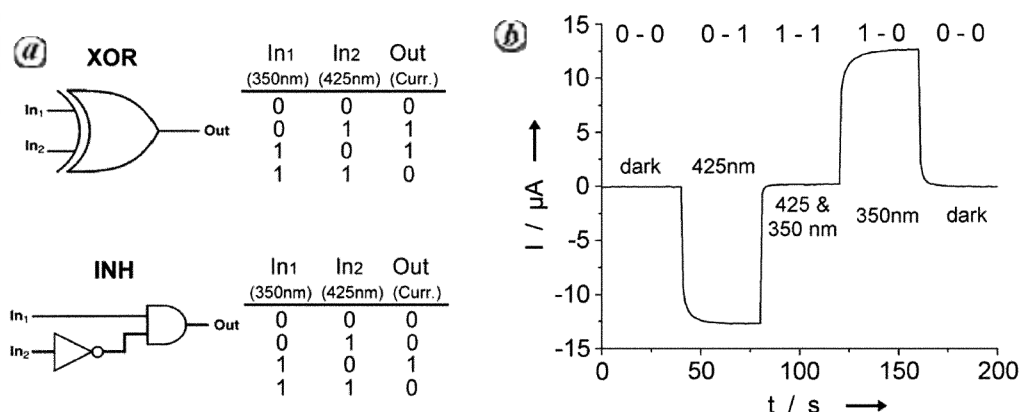
Figure 22. XOR and INH logic gates based on the $TiO_2/[Ru_3O(Ac)_6(py)_2(pzCO_2H)]PF_6$ photoelectrochemical cell, (*a*) truth tables, (*b*) input–output responses.

The photoaction spectrum (Figure 20) of a cell assembled with the ruthenium cluster exhibits a maximum photocurrent around 350 nm, becoming null at 375 nm and then negative up to 600 nm, reaching a minimum at 410 nm where the absorption peak of the adsorbed cluster complex is localized.

Two major processes are driving the photocurrent in opposite directions, as illustrated in Figure 21. One is the direct absorption of light by the *n*-type TiO_2 layer and the second is the abstraction of electrons by the excited cluster complex. The first one is predominant at λ_{exc} <375 nm and the current tends to increase sharply as λ_{exc} decreases, but because of the glass filtering effect, a maximum is observed at 350 nm. This peak is the sole feature observed for non-sensitized nanocrystalline TiO_2 films. Above 375 nm the photocurrent becomes dependent on the excited state properties of the adsorbed dye. The adsorbed complex has a broad charge transfer band at 420 nm, coinciding with the negative peak in the photoaction spectrum. Electron injection from hot excited states are known to be responsible for the high efficiency of Grätzel cells, but this is the first report on electron injection in the reverse direction, i.e. from the TiO_2 film to the excited dye sensitizer. The mechanism involved is

depicted in Figure 21, involving the reductive quenching of C* by the TiO_2 layer followed by reduction of I_2 to I^- by the cluster species and migration of electrons to the counter electrode in order to close the circuit.

Such photoelectrochemical response can be readily exploited in the design of a XOR logic gate, which is difficult to be emulated at the molecular scale[263]. The photocurrent output (O) obtained by using 350 and 425 nm light as inputs (I1 and I2 respectively) are shown in Figure 22. When I1 and I2 are equal to 0 (no light, 0 – 0) no photocurrent is generated (O = 0). When λ_{exc} = 425 nm (0 – 1), a cathodic photocurrent is recorded and O = 1. An anodic photocurrent is recorded when 350 nm light hits the cell (1 – 0) and again O = 1. However, if the cell is irradiated simultaneously with both λ_{exc} (350 and 420 nm, 1 – 1), no net current flows since they are canceled out (O = 0). The truth table matches the one for the XOR gate. Once the binary logic is based on threshold values[229], the INH gate also can be obtained simply by changing the intensity or the λ_{exc} of one of the inputs in such a way to decrease the absolute output signal and establish a threshold in between O1 and O2. For example, one can set up 7 and 13 μA as the outputs and 10 μA as threshold to realize the INH logic gate.

Concluding remarks

By exploiting the strategies of supramolecular chemistry, versatile functional nanomaterials have been designed, conveying the remarkable characteristics of the several building blocks, such as their electronic, optical and chemical properties. In particular, coordination chemistry has provided effective self-assembly strategies for molecular materials, based on specific metal-ligand affinity and stereochemistry. From the several supramolecular porphyrins and porphyrazines, metal-clusters and metal-polyimines focused on this article, an exciting field of investigation can be envisioned, covering a wide range of applications in catalysis, sensors and molecular devices.

1. Lehn, J.-M., *Supramolecular Chemistry: Concepts and Perspectives*, VCH, New York, 1995.
2. Atwood, J. L., Davies, J. E. D., Macnicol, D. D., Vögtle, F. and Lehn, J.-M., *Comprehensive Supramolecular Chemistry* (ed. Lehn, J.-M.), Pergamon, New York, 1996.
3. Araki, K. and Toma, H. E., *N4–Macrocyclic Metal Complexes* (eds Zagal, J., Bedioui, F. and Dodelet, J. P.), Springer, New York, 2006, pp. 255–314.
4. Balzani, V., Venturi, M. and Credi, A., *Molecular Devices and Machines – A Journey into the Nanoworld*, Wiley-VCH Verlag Gmbh and Co, Weinheim, 2003.
5. Ballardini, R., Balzani, V., Credi, A., Gandolfi, M. T. and Venturi, M., Artificial molecular-level machines: Which energy to make them work? *Acc. Chem. Res.*, 2001, **34**, 445–455.
6. Credi, A., Balzani, V., Langford, S. J. and Stoddart, J. F., Logic operations at the molecular level. An XOR gate based on a molecular machine. *J. Am. Chem. Soc.*, 1997, **119**, 2679–2681.
7. Hipps, K. W., Molecular electronics – It's all about contacts. *Science*, 2001, **294**, 536–537.
8. Ratner, M., Molecular electronics – Pushing electrons around. *Nature*, 2000, **404**, 137–138.
9. Anson, F. C., Shi, C. N. and Steiger, B., Novel multinuclear catalysts for the electroreduction of dioxygen directly to water. *Acc. Chem. Res.*, 1997, **30**, 437–444.
10. Barigelletti, F., Flamigni, L., Balzani, V., Collin, J. P. and Sauvage, J. P., Sour a luminescence properties of rigid, rod-like, dichromophoric species – dinuclear Ru–Os terpyridine-type complexes with 2.4 Nm metal-to-metal distance. *New J. Chem.*, 1995, **19**, 793–798.
11. Flamigni, L., Barigelletti, F., Armaroli, N., Collin, J. P., Sauvage, J. P. and Williams, J. A. G., Photoinduced processes in highly coupled multicomponent arrays based on a ruthenium(II)bis(terpyridine) complex and porphyrins. *Chemistry – a Eur. J.*, 1998, **4**, 1744–1754.
12. Mayer, I., Nunes, G. S., Toma, H. E. and Araki, K., Steric and catalytic effects in tetraruthenated manganese porphyrins. *Eur. J. Inorg. Chem.*, 2006, 850–856.
13. Winnischofer, H., Formiga, A. L. B., Nakamura, M., Toma, H. E., Araki, K. and Nogueira, A. F., Conduction and photoelectrochemical properties of monomeric and electropolymerized tetraruthenated porphyrin films. *Photochem. Photobiol. Sci.*, 2005, **4**, 359–366.
14. Drain, C. M., Nifiatis, F., Vasenko, A. and Batteas, J. D., Porphyrin tessellation by design: Metal-mediated self-assembly of large arrays and tapes. *Angew. Chemie. Int. Edn.*, 1998, **37**, 2344–2347.
15. Fujita, M., Aoyagi, M., Ibukuro, F., Ogura, K. and Yamaguchi, K., Made-to-order assembling of [2]catenanes from palla-
dium(II)-linked rectangular molecular boxes. *J. Am. Chem. Soc.*, 1998, **120**, 611–612.
16. Toma, H. E. and Araki, K., Supramolecular assemblies of ruthenium complexes and porphyrins. *Coord. Chem. Rev.*, 2000, **196**, 307–329.
17. Toma, H. E., Araki, K., Alexiou, A. D. P., Nikolaou, S. and Dovidauskas, S., Monomeric and extended oxo-centered triruthenium clusters. *Coord. Chem. Rev.*, 2001, **219**, 187–234.
18. Balzani, V. and Scandola, F., *Supramolecular Photochemistry*, Ellis Horwood, Chichester, UK, 1991.
19. Schlicke, B., Belser, P., De Cola, L., Sabbioni, E. and Balzani, V., Photonic wires of nanometric dimensions. Electronic energy transfer in rigid rod-like Ru(bpy)(3)(2+)-(ph)(n)-Os(bpy)(3)(2+) compounds (ph = 1,4-phenylene; n = 3, 5, 7). *J. Am. Chem. Soc.*, 1999, **121**, 4207–4214.
20. Vogtle, F. *et al.*, Dendrimers with a photoactive and redox-active [Ru(bpy)(3)](2+)-type core: Photophysical properties, electrochemical behaviour, and excited-state electron-transfer reactions. *J. Am. Chem. Soc.*, 1999, **121**, 6290–6298.
21. Belser, P., Bernhard, S., Blum, C., Beyeler, A., De Cola, L. and Balzani, V., Molecular architecture in the field of photonic devices. *Coord. Chem. Rev.*, 1999, **192**, 155–169.
22. Juris, A., Balzani, V., Barigelletti, F., Campagna, S., Belser, P., and Vonzelewsky, A., Ru(II) polypyridine complexes – Photophysics, photochemistry, electrochemistry, and chemiluminescence. *Coord. Chem. Rev.*, 1988, **84**, 85–277.
23. Camera, S. G. and Toma, H. E., Photophysical behavior of molecular dyads and triad comprising tris(bipyrazine)ruthenium(II), bis(bipyridine)chlororuthenium(II) and pentacyanoferrate(II) complexes. *J. Photochem. Photobiol. A – Chem.*, 2002, **151**, 57–65.
24. Toma, H. E. and Lever, A. B. P., Spectroscopic and kinetic studies on a series of dinuclear to heptanuclear tris(bipyrazine) ruthenium(II)–pentacyanoferrate(II) complexes in aqueous solution. *Inorg. Chem.*, 1986, **25**, 176–181.
25. Toma, H. E., Auburn, P. R., Dodsworth, E. S., Golovin, M. N. and Lever, A. B. P., Binding of pentaammineruthenium(II) residues to the tris(bipyrazine)ruthenium(II) cation. *Inorg. Chem.*, 1987, **26**, 4257–4263.
26. Toma, H. E., Santos, P. S. and Lever, A. B. P., Resonance Raman spectra of the heptanuclear [Ru(bpz)3(Ru(NH3)5)6]14$^+$ complex – Excitation profiles for 3 overlapping metal-to-ligand charge-transfer bands. *Inorg. Chem.*, 1988, **27**, 3850–3853.
27. Balzani, V., Bergamini, G., Marchioni, F. and Ceroni, P., Ru(II)–bipyridine complexes in supramolecular systems, devices and machines. *Coord. Chem. Rev.*, 2006, **250**, 1254–1266.
28. Tanaka, H., Yajima, T., Matsumoto, T., Otsuka, Y. and Ogawa, T., Porphyrin molecular nanodevices wired using single-walled carbon nanotubes. *Adv. Mater.*, 2006, **18**, 1411–1418.
29. Ozawa, H., Kawao, M., Tanaka, H. and Ogawa, T., Synthesis of end-functionalized pi-conjugated porphyrin oligomers. *Tetrahedron*, 2006, **62**, 4749–4755.
30. Sato, H., Tsutsumi, O., Takeda, K., Tanaka, H. and Ogawa, T., Simple preparation method for supramolecular porphyrin arrays on mica using air–water interface. *Jap. J. Appl. Phys.*, 2006, **45**, 2324–2327.
31. Latos-Grazynski, L., Rachlewicz, K. and Wojaczynski, J., Novel routes for the modification of iron porphyrins. *Coord. Chem. Rev.*, 1999, **192**, 109–125.
32. Imamura, T. and Fukushima, K., Self-assembly of metallopyridylporphyrin oligomers. *Coord. Chem. Rev.*, 2000, **198**, 133–156.
33. Sanders, J. K. M., in *The Porphyrin Handbook* (eds Kadish, K. M., Smith, K. M. and Guilard, R.), Academic Press, New York, 2000, pp. 347–368.
34. Chambron, J. C., Heitz, V. and Sauvage, J. P., in *The Porphyrin Handbook* (eds Kadish, K. M., Smith, K. M. and Guilard, R.), Academic Press, New York, 2000, pp 1–42.

35. Baldini, L. and Hunter, C. A., *Adv. Inorg. Chem.*, 2002, **53**, 213–259.

36. Prodi, A., Indelli, M. T., Kleverlaan, C. J., Alessio, E. and Scandola, F., Energy transfer pathways in pyridylporphyrin metal adducts and side-to-face arrays. *Coord. Chem. Rev.*, 2002, **229**, 51–58.

37. Toma, H. E. and Araki, K., Synthesis and properties of a new polymetallated iron porphyrin, *J. Chem. Res.– S*, 1990, 82–83.

38. Araki, K. and Toma, H. E., Synthesis and electrochemical behavior of a tetrametallated iron porphyrin, *Inorg. Chim. Acta*, 1991, **179**, 293–296.

39. Araki, K. and Toma, H. E., Spectroeletrochemical analysis of overlapping redox processes in a tetrametallated iron porphyrin. *J. Electroanal. Chem.*, 1991, **297**, 301–307.

40. Araki, K. and Toma, H. E., Synthesis and characterization of a multibridged porphyrin complex containing peripheral bis(bipyridine)ruthenium(II) groups. *J. Coord. Chem.*, 1993, **30**, 9–17.

41. Araki, K. and Toma, H. E., Luminescence, spectroelectrochemistry and photoelectrochemical properties of a tetraruthenated zinc porphyrin. *J. Photochem. Photobiol. A – Chem.*, 1994, **83**, 245–250.

42. Angnes, L., Azevedo, C. M. N., Araki, K. and Toma, H. E., Electrochemical detection of NADH and dopamine in flow analysis based on tetraruthenated porphyrin modified electrodes. *Anal. Chim. Acta*, 1996, **329**, 91–95.

43. Onuki, J., Ribas, A. V., Medeiros, M. H. G., Araki, K., Toma, H. E., Catalani, L. H. and Di Mascio, P., Supramolecular cationic tetraruthenated porphyrin induces single-strand breaks and 8-oxo-7,8-dihydro-2'-deoxyguanosine formation in DNA in the presence of light. *Photochem. Photobiol.*, 1996, **63**, 272–277.

44. Ravanat, J. L., Cadet, J., Araki, K., Toma, H. E., Medeiros, M. H. G. and Di Mascio, P., Supramolecular cationic tetraruthenated porphyrin and light-induced decomposition of 2'-deoxyguanosine predominantly via a singlet oxygen-mediated mechanism. *Photochem. Photobiol.*, 1998, **68**, 698–702.

45. Araki, K., Dovidauskas, S., Winnischofer, H., Alexiou, A. D. P. and Toma, H. E., A new highly efficient tetra-electronic catalyst based on a cobalt porphyrin bound to four mu(3)-oxo-ruthenium acetate clusters. *J. Electroanal. Chem.*, 2001, **498**, 152–160.

46. Engelmann, F. M., Losco, P., Winnischofer, H., Araki, K. and Toma, H. E., Synthesis, electrochemistry, spectroscopy and photophysical properties of a series of meso-phenylpyridylporphyrins with one to four pyridyl rings coordinated to [Ru(bipy)(2)Cl](+) groups. *J. Porph. Phthalocyanines*, 2002, **6**, 33–42.

47. Winnischofer, H., Lima, S. D., Araki, K. and Toma, H. E., Electrocatalytic activity of a new nanostructured polymeric tetraruthenated porphyrin film for nitrite detection. *Anal. Chim. Acta*, 2003, **480**, 97–107.

48. Araki, K. *et al.*, Enhanced electrochemical and electrocatalytic activity of a new supramolecular manganese-porphyrin species containing four bis(bipyridine)(aqua)ruthenium(II) complexes. *J. Electroanal. Chem.*, 2004, **562**, 145–152.

49. Nogueira, A. F. *et al.*, Photoelectrochemical properties of supramolecular species containing porphyrin and ruthenium complexes on TiO₂ films. *Photochem. Photobiol. Sci.*, 2004, **3**, 56–62.

50. Nogueira, A. F. *et al.*, Sensitization of TiO₂ by supramolecules containing zinc porphyrins and ruthenium–polypyridyl complexes. *Inorg. Chem.*, 2004, **43**, 396–398.

51. Winnischofer, H., Otake, V. Y., Dovidauskas, S., Nakamura, M., Toma, H. E. and Araki, K., Supramolecular tetracluster–cobalt porphyrin: a four-electron transfer catalyst for dioxygen reduction. *Electrochim. Acta*, 2004, **49**, 3711–3718.

52. Nunes, G. S., Mayer, I., Toma, H. E. and Araki, K., Kinetics and mechanism of cyclohexane oxidation catalyzed by supramolecular manganese(III) porphyrins. *J. Catal.*, 2005, **236**, 55–61.

53. Quintino, M., Winnischofer, H., Nakamura, M., Araki, K., Toma, H. E. and Angnes, L., Amperometric sensor for glucose based on electrochemically polymerized tetraruthenated nickel-porphyrin. *Anal. Chim. Acta*, 2005, **539**, 215–222.

54. Toyama, M. M., Araki, K. and Toma, H. E., Absorption and luminescence spectra of tetra(3-pyridyl)porphyrazine: A convergent spectroscopic method for the elucidation of association reactions in solution. *Spectrosc. Lett.*, 1998, **31**, 1065–1074.

55. Toyama, M. M., Franco, M., Catalani, L. H., Araki, K. and Toma, H. E., Spectroelectrochemical and photophysical properties of a (3,4-pyridyl)porphyrazine supermolecule containing four [Ru(bipy)(2)Cl](+) groups. *J. Photochem. Photobiol. A – Chem.*, 1998, **118**, 11–17.

56. Toyama, M. M., Demets, G. J. F., Araki, K. and Toma, H. E., Highly conductive electrostatically assembled porphyrazine films. *Electrochem. Commun.*, 2000, **2**, 749–753.

57. Toma, S. H. and Toma, H. E., Versatile electrochromic displays based on TiO₂ nanoporous films modified with triruthenium clusters. *Electrochem. Commun.*, 2006, **8**, 1628–1632.

58. Nunes, G. S., Alexiou, A. D. P., Araki, K., Formiga, A. L. B., Rocha, R. C. and Toma, H. E., Proton-coupled redox chemistry, oxidative reactivity, and electronic characterization of aqua-, hydroxo-, and oxo-triruthenium clusters. *Eur. J. Inorg. Chem.*, 2006, 1487–1495.

59. Toma, S. H., Nikolaou, S., Tomazela, D. M., Eberlin, M. N. and Toma, H. E., Synthesis, spectroscopy, tandem mass spectrometry, and electrochemistry of the linearly bridged {trans-1,4-bis [2(4-pyridyl)ethenyl]-benzene}-{Ru3O(acetate)(6)(py)(2)} cluster. *Inorg. Chim. Acta*, 2004, **357**, 2253–2260.

60. Toma, H. E., Alexiou, A. D. P. and Dovidauskas, S., Extended electronic interactions in a triangular mu-oxotriruthenium acetate cluster containing nitric oxide. *Eur. J. Inorg. Chem.*, 2002, 3010–3017.

61. Nikolaou, S. and Toma, H. E., Synthesis, spectroscopy and electrochemistry of a mu-oxo-triruthenium cluster containing a bridged bis(2,2'-bipyridyl)ruthenium(II) moiety. *Polyhedron*, 2001, **20**, 253–259.

62. Nikolaou, S., Uemi, M. and Toma, H. E., Total assignment of H-1 and C-13 NMR spectra of a bridged triruthenium cluster-polypyridine dimer based on 2D (COSY, HMQC, and HMBC) techniques. *Spectrosc. Lett.*, 2001, **34**, 267–277.

63. Toma, H. E. and Nikolaou, S., Self-assembly of a supramolecular cyclic polymer containing pyrazine bridged trinuclear mu-oxo-ruthenium-acetate clusters. *J. Chem. Res. - S*, 2000, 326–327.

64. Alexiou, A. D. P., Dovidauskas, S. and Toma, H. E., Properties and applications of trinuclear ruthenium carboxylate clusters. *Quimica Nova*, 2000, **23**, 785–793.

65. Alexiou, A. D. P. and Toma, H. E., NMR spectroscopic correlations for a series of triangular alpha-oxoruthenium acetate clusters containing substituted pyridine ligands. *J. Chem. Res.– S*, 1997, 338–339.

66. Araujo, J., Nikolaou, S., Alexiou, A. D. P. and Toma, H. E., Synthesis of a trinuclear ruthenium cluster containing pyridine and 4-acetylpyridine ligands and its immobilization on functionalized silica. *Monatshefte Chemie*, 1997, **128**, 759–766.

67. Toma, H. E. and Alexiou, A. D. P., Synthesis and characterization of a dodecanuclear ruthenium pyrazine cluster. *J. Braz. Chem. Soc.*, 1995, **6**, 267–270.

68. Toma, H. E. and Alexiou, A. D. P., Nuclear magnetic resonance and spectroelectrochemical characterization of a supramolecular tetrameric ruthenium cluster. *J. Chem. Res. – S*, 1995, 134–135.

69. Toma, H. E. and Olive, M. A. L., Spectroelectrochemical and kinetic studies on the interaction of ruthenium-edta with a trinuclear ruthenium acetate cluster containing aminopyrazine ligands. *Polyhedron*, 1994, **13**, 2647–2652.

70. Alexiou, A. D. P. and Toma, H. E., Electrochemical parametrization of ruthenium cluster redox potentials. *J. Chem. Res. – S*, 1993, 464–465.

71. Toma, H. E., Matsumoto, F. M. and Cipriano, C., Spectroelectro-chemistry of the hexanuclear ruthenium-acetate-pyrazine penta-cyanoferrate(II) cluster and of its modified nickel electrode in aqueous solution. *J. Electroanal. Chem.*, 1993, **346**, 261–270.

72. Toma, H. E. and Alexiou, A. D. P., Dynamic electrochemical behaviour of a trinuclear m-oxo ruthenium acetate cluster containing pyridine and dimethylsulphoxide ligands. *Electrochim. Acta*, 1993, **38**, 975–1002.

73. Toma, H. E. and Cipriano, C., Synthesis and spectroscopic characterization of trinuclear ruthenium-acetate-pyrazine clusters. *Monatshefte Chemie*, 1989, **120**, 815–820.

74. Toma, H. E. and Cipriano, C., Spectroelectrochemistry and cyclic voltammetry of the trinuclear ruthenium-hexaacetate-tris (pyrazine) cluster. *J. Electroanal. Chem.*, 1989, **263**, 313–322.

75. Toma, H. E. and Cunha, C. J., Spectroelectrochemical behavior of the trinuclear ruthenium-acetate-isonicotinamide cluster. *Can. J. Chem.–*1989, **67**, 1632–1635.

76. Toma, H. E., Santos, P. S. and Cipriano, C., Electronic and resonance Raman spectra of the hexanuclear cluster [Ru3O(acetate)6 (pyrazine)Ru(NH3)5)3]6+. *Spectrosc. Lett.*, 1988, **21**, 909–918.

77. Araki, K., Lima, S. D. and Winnischofer, H., Thin molecular films of supramolecular porphyrins. *Anais Acad. Brasileira Ciencias*, 2000, **72**, 27–32.

78. Toma, H. E., Araki, K. and Silva, E. O., Synthesis and characterization of a novel dodecanuclear porphyrin ruthenium cluster. *Monatshefte Chemie*, 1998, **129**, 975–984.

79. Dovidauskas, S., Araki, K. and Toma, H. E., Electrochemical and binding properties of a meso-tetra(4-pyridyl)porphyrinatozinc supermolecule containing four mu(3)-oxo-triruthenium acetate clusters. *J. Porph. Phthalocyanines*, 2000, **4**, 727–735.

80. Dovidauskas, S., Toma, H. E., Araki, K., Sacco, H. C. and Iamamoto, Y., (5,10,15,20-Tetra(4-pyridil)porphinato)manganes(III) acetate modified by four mu(3)-oxo-triruthenium acetate clusters: synthesis, characterization, electrochemical behavior and catalytic activity. *Inorg. Chim. Acta*, 2000, **305**, 206–213.

81. Araki, K., Angnes, L., Azevedo, C. M. N. and Toma, H. E., Electrochemistry of a tetraruthenated cobalt porphyrin and its use in modified electrodes as sensors of reducing analytes. *J. Electroanal. Chem.*, 1995, **397**, 205–210.

82. Araki, K., Araujo, A. L., Toyama, M. M., Franco, M., Azevedo, C. M. N., Angnes, L. and Toma, H. E., Spectroscopic and electrochemical study of a tetrapyridylporphyrin modified with four bis-(1,10–phenanthroline)chlororuthenium(II) complexes. *J. Porph. Phthalocyanines*, 1998, **2**, 467–472.

83. Araki, K. and Toma, H. E., Electrochemistry of a tetraruthenated iron porphyrin and its electrostatically assembled bilayered films. *Electrochim. Acta*, 1999, **44**, 1577–1583.

84. Araki, K., Angnes, L. and Toma, H. E., Rectifying properties and photoduenductivity of tetraruthenated nickel porphyrin films. *Adv. Mat.*, 1995, **7**, 554–559.

85. Araki, K., Wagner, M. J. and Wrighton, M. S., Layer-by-layer growth of electrostatically assembled multilayer porphyrin films. *Langmuir*, 1996, **12**, 5393–5398.

86. Azevedo, C. M. N., Araki, K., Toma, H. E. and Angnes, L., Determination of sulfur dioxide in wines by gas-diffusion flow injection analysis utilizing modified electrodes with electrostatically assembled films of tetraruthenated porphyrin. *Anal. Chim. Acta*, 1999, **387**, 175–180.

87. Azevedo, C. M. N., Araki, K., Angnes, L. and Toma, H. E., Electrostatically assembled films for improving the properties of tetraruthenated porphyrin modified electrodes. *Electroanalysis*, 1998, **10**, 467-471.

88. Quintino, M. S. M., Araki, K., Toma, H. E. and Angnes, L., Batch injection analysis utilizing modified electrodes with tetraruthenated porphyrin films for acetaminophen quantification. *Electroanalysis*, 2002, **14**, 1629–1634.

89. Calvo, E. J., Danilowicz, C. B. and Wolosiuk, A., Supramolecular multilayer structures of wired redox enzyme electrodes. *Chemphyschem.*, 2005, **7**, 1800–1806.

90. Calvo, E. J. and Wolosiuk, A., Wiring enzymes in nanostructures built with electrostatically self-assembled thin films. *Chemphyschem*, 2005, **6**, 43–47.

91. Vago, M., Campodall'Orto, V., Rezzano, I., Forzani, E. S. and Calvo, E. J., Metalloporphyrin electropolymerization: electrochemical quartz crystal microgravimetric studies. *J. Electroanal. Chem.*, 2004, **566**, 177–185.

92. Calvo, E. J. and Wolosiuk, A., Supramolecular architectures of electrostatic self-assembled glucose oxidase enzyme electrodes. *Chemphyschem*, 2004, **5**, 235–239.

93. Calvo, E. J., Danilowicz, C. and Wolosiuk, A., Molecular 'wiring' enzymes in organized nanostructures. *J. Am. Chem. Soc.*, 2002, **124**, 2452–2453.

94. da Rocha, J. R. C., Demets, G. J. F., Bertotti, M., Araki, K. and Toma, H. E., Charge transfer at electrostatically assembled tetraruthenated porphyrin modified electrodes. *J. Electroanal. Chem.*, 2002, **526**, 69–76.

95. da Rocha, J. R. C., Angnes, L., Bertotti, M., Araki, K. and Toma, H. E., Amperometric detection of nitrite and nitrate at tetraruthenated porphyrin-modified electrodes in a continuous-flow assembly. *Ana. Chim. Acta*, 2002, **452**, 23–28.

96. Denisevich, P., Abruna, H. D., Leidner, C. R., Meyer, T. J. and Murray, R. W., Electropolymerization of vinylpyridine and vinylbipyridine complexes of iron and ruthenium – homopolymers, copolymers, reactive polymers. *Inorg. Chem.*, 1982, **21**, 2153–2161.

97. Deronzier, A., Devaux, R., Limosin, D. and Latour, J. M., Poly(pyrrole-metallotetraphenylporphyrin)-modified electrodes. *J. Electroanal. Chem.*, 1992, **324**, 325–337.

98. Younathan, J., Wood, K. S. and Meyer, T. J., Electropolymerization porphyrin. *Inorg. Chem.*, 1992, **31**, 3280–3286.

99. Bommarito, S. L., Lowerybretz, S. P. and Abruna, H. D., Homogeneous and heterogeneous synthesis of redox polymers and copolymers of [M(4-vinyl-4′-methyl-2,2′-bipyridine)3](PF6)2 (M = Ru, Os). *Synlett*, 1993, 375–385.

100. Hayon, J., Raveh, A. and Bettelheim, A., Electropolymerization porphyrin. *J. Electroanal. Chem.* 1993, **359**, 209–214.

101. Deronzier, A. and Moutet, J. C., Polypyrrole films containing metal complexes: Syntheses and applications. *Coord. Chem. Rev.*, 1996, **147**, 339–371.

102. Cosnier, S., Galland, B. and Innocent, C., New electropolymerizable amphiphilic viologens for the immobilization and electrical wiring of a nitrate reductase. *J. Electroanal. Chem.*, 1997, **433**, 113–119.

103. Shimidzu, T., Approaches to ultimate functional polymer materials. *Polymers Adv. Technol.*, 1997, **8**, 275–280.

104. Kuester, S. N., McGuire, M. M. and Drew, S. M., Electrochemically initiated polymerization of zinc(II)5-vinyl-10,15,20-triphenylporphyrin. *J. Electroanal. Chem.*, 1998, **452**, 13–18.

105. Storrier, G. D., Takada, K. and Abruna, H. D., Catechol-pendant terpyridine complexes: Electrodeposition studies and electrocatalysis of NADH oxidation. *Inorg. Chem.*, 1999, **38**, 559–565.

106. Bruti, E. M., Giannetto, M., Mori, G. and Seeber, R., Electropolymerization of tetrakis(o-aminophenyl)porphyrin and relevant transition metal complexes from aqueous solution. The resulting modified electrodes as potentiometric sensors. *Electroanalysis*, 1999, **11**, 565–572.

107. Schaferling, M. and Bauerle, P., Electrochemical properties of porphyrin-functionalized polythiophenes. *Synthetic Metals*, 2001, **119**, 289–290.

108. Bommarito, S. L., Lowerybretz, S. P. and Abruna, H. D., Synthesis and characterization of redox copolymers of [Ru(4-vinyl-4′-methyl-2,2′-bipyridine)3]2+ and [Os(4-vinyl-4′-methyl-2,2′-Bipyridine)3]2+ – unusual energy-transfer dynamics. *Inorg. Chem.*, 1992, **31**, 502–507.

109. Takada, K., Storrier, G. D., Pariente, F. and Abruna, H. D., EQCM studies of the redox processes during and after electropolymerization of films of transition–metal complexes of vinylterpyridine. *J. Phys. Chem. B*, 1998, **102**, 1387–1396.

110. Takada, K., Storrier, G. D., Goldsmith, J. I. and Abruna, H. D., Electrochemical and adsorption properties of PAMAM dendrimers surface-functionalized with polypyridyl cobalt complexes. *J. Phys. Chem.*, 2001, **B105**, 2404–2411.

111. Diab, N. and Schuhmann, W., Electropolymerized manganese porphyrin/polypyrrole films as catalytic surfaces for the oxidation of nitric oxide. *Electrochim. Acta*, 2001, **47**, 265–273.

112. Diab, N., Oni, J., Schulte, A., Radtke, I., Blochl, A. and Schuhmann, W., Pyrrole functionalised metalloporphyrins as electrocatalysts for the oxidation of nitric oxide. *Talanta*, 2003, **61**, 43–51.

113. Araki, K., Endo, H., Masuda, G. and Ogawa, T., Bridging nanogap electrodes by in situ electropolymerization of a bis(terthiophenylphenanthroline)ruthenium complex. *Chemistry–A Eur. J.*, 2004, **10**, 3331–3340.

114. Maranhao, S. L. A., Guedes, I. C., Anaissi, F. J., Toma, H. E. and Aoki, I. V., Electrochemical and corrosion studies of poly (nickel-tetraaminophthalocyanine) on carbon steel. *Electrochim. Acta*, 2006, **52**, 519–526.

115. Fussa-Rydel, O., Zhang, H.-T., Hupp, J. T. and Leidner, C. R., Electrochemical assembly of metallopolymeric films via reaction of coordinated 5-chlorophenanthroline. *Inorg. Chem.*, 1989, **28**, 1533–1537.

116. Andrieux, C. P. and Saveant, J. M., Electron-transfer through redox polymer films. *J. Electroanal. Chem.*, 1980, **111**, 377–381.

117. Andrieux, C. P., Haas, O. and Saveant, J. M., Catalysis of electrochemical reactions at redox polymer coated electrodes – mediation of the Fe(III)/Fe(II) oxidoreduction by a polyvinylpyridine polymer containing coordinatively attached bisbipyridine chlororuthenium redox centers. *J. Am. Chem. Soc.*, 1986, **108**, 8175–8182.

118. Andrieux, C. P., Hapiot, P. and Saveant, J. M., Fast chemical steps coupled with outer-sphere electron transfers – application of fast scan voltammetry at ultramicroelectrodes to the cleavage of aromatic halide anion radicals in the microsecond lifetime range. *J. Phys. Chem.*, 1988, **92**, 5987–5992.

119. Balzani, V., Credi, A., Raymo, F. M. and Stoddart, J. F., Artificial molecular machines. *Angew. Chemie-Int. Ed.*, 2000, **39**, 3349–3391.

120. Merkle, R. C., Molecular building blocks and development strategies for molecular nanotechnology. *Nanotechnology*, 2000, **11**, 89–99.

121. Badjic, J. D., Balzani, V., Credi, A., Silvi, S. and Stoddart, J. F., A molecular elevator. *Science*, 2004, **303**, 1845–1849.

122. Sauvage, J. P., Transition metal-containing rotaxanes and catenanes in motion: Toward molecular machines and motors. *Acc. Chem. Res.*, 1998, **31**, 611–619.

123. Chia, S. Y., Cao, J. G., Stoddart, J. F. and Zink, J. I., Working supramolecular machines trapped in glass and mounted on a film surface. *Angew. Chem–Int. Ed.*, 2001, **40**, 2447–2450.

124. Stoddart, J. F., Molecular machines. *Acc. Chem. Res.*, 2001, **34**, 410–411.

125. Balzani, V. and Juris, A., Photochemistry and photophysics of Ru(II)-polypyridine complexes in the Bologna group. From early studies to recent developments. *Coord. Chem. Rev.*, 2001, **211**, 97–115.

126. Winnischofer, H., Toma, H. E. and Araki, K., Polymetallated porphyrin ultrathin films as transducing elements for molecular devices and logic gates. *J. Nanosci. Nanotechnol.*, 2006, **6**, 1701–1709.

127. Furtado, L. F. O., Alexiou, A. D. P., Goncalves, L., Toma, H. E. and Araki, K., TiO₂-based light-driven XOR/INH logic gates. *Angew. Chem.-Int. Ed.*, 2006, **45**, 3143–3146.

128. Toma, H. E., Molecular materials and devices: Developing new functional systems based on the coordination chemistry approach. *J. Braz. Chem. Soc.*, 2003, **14**, 845–869.

129. Toma, H. E., Supramolecular chemistry and technology. *Anais Acad. Brasileira Ciencias*, 2000, **72**, 5–25.

130. Denti, G. *et al.*, Luminescent and redox-reactive building blocks for the design of photochemical molecular devices: mono, di, tri and tetranuclear ruthenium(II) polypyridine complexes. *Inorg. Chem.*, 1990, **29**, 4750–4758.

131. Hung, S. C. *et al.*, Kinetics of multistep photoinitiated electron-transfer reactions in a molecular triad. *J. Photochem. Photobiol A – Chem.*, 1994, **77**, 207–216.

132. Lehn, J. M., Supramolecular chemistry scope and perspectives – molecules, supermolecules, molecular devices. *J. Inclusion Phenom.*, 1988, **6**, 351.

133. Pease, A. R. and Stoddart, J. F., *Molecular Machines and Motors, in Structure and Bonding* (ed. Sauvage, J.-P), Springer, 2001, pp. 189–236.

134. Balzani, V., Credi, A. and Venturi, M., The bottom-up approach to molecular-level devices and machines. *Chem. – A Eur. J.*, 2002, **8**, 5524–5532.

135. Whitesides, G. M. and Grzybowski, B., Self-assembly at all scales. *Science*, 2002, **295**, 2418–2421.

136. Balzani, V., Campagna, S., Denti, G., Juris, A., Serroni, S. and Venturi, M., Bottom up strategy to obtain luminescent and redox active metal complexes of nanometric dimensions. *Coord. Chem. Rev.*, 1994, **132**, 1–13.

137. Oliveri, C. G., Heo, J., Nguyen, S. T., Mirkin, C. A. and Wawrzak, Z., A convergent coordination chemistry-based approach to dissymmetric macrocyclic cofacial porphyrin complexes. *Inorg. Chem.*, 2007, **46**, 7716–7718.

138. Kuwabara, J., Stern, C. L. and Mirkin, C. A., A coordination chemistry approach to a multieffector enzyme mimic. *J. Am. Chem. Soc.*, 2007, **129**, 10074–10079.

139. Cheng, M. M. C. *et al.*, Nanotechnologies for biomolecular detection and medical diagnostics. *Curr. Op. Chem. Biol.*, 2006, **10**, 11–19.

140. Legnani, C., Reyes, R., Cremona, M., Bagatin, I. A. and Toma, H. E., Tunable blue organic light emitting diode based on aluminum calixarene supramolecular complex. *Appl. Phys. Lett.*, 2004, **85**, 10–12.

141. Lvov, Y., Ariga, K., Ichinose, I. and Kunitake, T., Assembly of multicomponent protein films by means of electrostatic layer-by-layer adsorption. *J. Am. Chem. Soc.*, 1995, **117**, 6117–6123.

142. da Silva, B. A., Antunes, P. A., Pasquini, D., Curvelo, A. A. S., Aroca, R. F., Riul, A. and Constantino, C. J. L., Nanostructured films employed as sensing units in an 'electronic tongue' system. *J. Nanosci. Nanotechnol.*, 2007, 7, 510–514.

143. Constantino, C. J. L. *et al.*, Nanostructured films of perylene derivatives: High performance materials for taste sensor applications. *Sensor Lett.*, 2004, **2**, 95–101.

144. de Melo, C. P., Neto, B. B., de Lima, E. G., de Lira, L. F. B. and de Souza, J. E. G., Use of conducting polypyrrole blends as gas sensors. *Sensors Actuators B – Chem.*, 2005, **109**, 348–354.

145. Riul, A., de Sousa, H. C., Malmegrim, R. R., dos Santos, D. S., Carvalho, A., Fonseca, F. J., Oliveira, O. N. and Mattoso, L. H. C., Wine classification by taste sensors made from ultra-thin films and using neural networks. *Sensors Actuators B – Chem.*, 2004, **98**, 77–82.

146. dos Santos, D. S., Riul, A., Malmegrim, R. R., Fonseca, F. J., Oliveira, O. N. and Mattoso, L. H. C., A layer-by-layer film of chitosan in a taste sensor application. *Macromol. Biosci.*, 2003, **3**, 591–595.

147. Riul, A., Malmegrim, R. R., Fonseca, F. J. and Mattoso, L. H. C., An artificial taste sensor based on conducting polymers. *Biosensors Bioelectronics*, 2003, **18**, 1365–1369.

148. Ferreira, M., Riul, A., Wohnrath, K., Fonseca, F. J., Oliveira, O. N. and Mattoso, L. H. C., High-performance taste sensor made from Langmuir–Blodgett films of conducting polymers and a ruthenium complex. *Anal. Chem.*, 2003, **75**, 953–955.

149. Riul, A., Soto, A. M. G., Mello, S. V., Bone, S., Taylor, D. M. and Mattoso, L. H. C., An electronic tongue using polypyrrole and polyaniline. *Synthetic Metals*, 2003, **132**, 109–116.

150. Riul, A. *et al.*, Artificial taste sensor: Efficient combination of sensors made from Langmuir–Blodgett films of conducting polymers and a ruthenium complex and self-assembled films of an azobenzene-containing polymer. *Langmuir*, 2002, **18**, 239–245.

151. de Souza, J. E. G., dos Santos, F. L., Barros-Neto, B., dos Santos, C. G. and de Melo, C. P., Polypyrrole thin films gas sensors. *Synthetic Metals*, 2001, **119**, 383–384.

152. Mayer, I., Eberlin, M. N., Tomazela, D. M., Toma, H. E. and Araki, K., Supramolecular conformational effects in the electrocatalytic properties of electrostatic assembled films of meso(3- and 4-pyridyl) isomers of tetraruthenated porphyrins. *J. Braz. Chem. Soc.*, 2005, **16**, 418–425.

153. Mayer, I. *et al.*, Study of the spectroscopic and electrochemical properties of tetraruthenated porphyrins by theoretical–experimental approach. *Inorg. Chim. Acta*, 2005, **358**, 2629–2642.

154. Mayer, I., Nakamura, K., Srinivasan, A., Furuta, H., Toma, H. E. and Araki, K., Spectroelectrochemical behavior of N-confused dioxohexaphyrins. *J. Porph. Phthalocyanines*, 2005, **9**, 813–820.

155. Araki, K. and Toma, H. E., Chemistry of supramolecular systems containing porphyrins and metal complexes. *Quimica Nova*, 2002, **25**, 962–975.

156. Mayer, I., Nakamura, M., Toma, H. E. and Araki, K., Multielectronic redox and electrocatalytic supramolecular films based on a tetraruthenated iron porphyrin. *Electrochim. Acta*, 2006, **52**, 263–271.

157. Mayer, I., Toma, H. E. and Araki, K., Electrocatalysis on tetraruthenated nickel and cobalt porphyrins electrostatic assembled films. *J. Electroanal. Chem.*, 2006, **590**, 111–119.

158. Quintino, M. S. M., Araki, K., Toma, H. E. and Angnes, L., Amperometric quantification of sodium metabisulfite in pharmaceutical formulations utilizing tetraruthenated porphyrin film modified electrodes and batch injection analysis. *Talanta*, 2006, **68**, 1281–1286.

159. Delfini, C. and Morsiani, M. G., Resistance to sulfur dioxide of malolactic trans of leuconostocoenos and lactobacillus SP isolated from wines. *Sci. Aliments*, 1992, **12**, 493–511.

160. Gomes, M. T., Rocha, T. A., Duarte, A. C. and Oliveira, J. P., Determination of sulfur dioxide in wine using a quartz crystal microbalance. *Anal. Chem.*, 1996, **68**, 1561–1564.

161. Ough, C. S., Determination of sulfur dioxide in grapes and wines, *J. Assoc. Official Anal. Chem.*, 1986, **69**, 5–7.

162. Ough, C. S., Kunkee, R. E., Vilas, M. R., Bordeu, E. and Huang, M. C., The interaction of sulfur dioxide, pH and dimethyl dicarbonate on the growth of *Saccharomyces cerevisiae* montrachet and leuconostocoenos MCW. *Am. J. Enology Viticult.*, 1988, **39**, 279–282.

163. Ough, C. S. and Crowell, E. A., Use of sulfur dioxide in winemaking. *J. Food Sci.*, 1987, **52**, 386–391.

164. Coker, L. E., Uses and analysis of sulfites in the corn wet milling industry. *J. Assoc. Official Anal. Chem.*, 1986, **69**, 8–10.

165. Moylan, J. G., Bowes, F. W. and Pappin, W. J., Evaluation of Monier–Williams and committee methods for bisulfite determination as used by the potato processing industry. *J. Assoc. Official Anal. Chem.*, 1986, **69**, 11–14.

166. Ough, C. S., Roessler, E. B. and Amerine, M. A., Effects of sulfur dioxide, temperature, time and closures on the quality of bottled dry white table wines. *Food Technol.*, 1960, **14**, 352–356.

167. Huang, Y. G., Ji, J. D. and Hou, Q. N., A study on carcinogenesis of endogenous nitrite and nitrosamine, and prevention of cancer. *Mutat. Res. – Fund. Mol. Mech. Mutagenesis*, 1996, **358**, 7–14.

168. Wolff, I. A. and Wassermae, A., Nitrates, nitrites, and nitrosamines. *Science*, 1972, **177**, 15–20.

169. Swann, P. F., Toxicology of nitrate, nitrite and nitrosamines. *J. Sci. Food Agric.*, 1975, **26**, 381–382.

170. Usher, C. D. and Telling, G. M., Analysis of nitrate andnitrite in foodstuffs – critical review. *J. Sci. Food Agric.*, 1975, **26**, 1793–1805.

171. Williams, A. E., Johnson, J. A., Lund, L. J. and Kabala, Z. J., Spatial and temporal variations in nitrate contamination of a rural aquifer, California. *J. Environ. Quality*, 1998, **27**, 1147–1157.

172. Williams, A. E., Lund, L. J., Johnson, J. A. and Kabala, Z. J., Natural and anthropogenic nitrate contamination of groundwater in a rural community, California. *Environ. Sci. Technol.*, 1998, **32**, 32–39.

173. Fontes, M. B. A., Angnes, L., Araki, K., Furlan, R. and Santiago-Aviles, J. J., A study of modified silicon based microelectrodes for nitric oxide detection. *Quim. Anal.*, 1999, **18**, 136–137.

174. Tan, M. X., Laibinis, P. E., Nguyen, S. T., Kesselman, J. M., Stanton, C. E. and Lewis, N. S., Principles and applications of semiconductor photoelectrochemistry. *Progr. Inorg. Chem.*, 1994, **41**, 21–144.

175. Oregan, B. and Gratzel, M., A low-cost, high-efficiency solar-cell based on dye-sensitized colloidal TiO_2 films. *Nature*, 1991, **353**, 737–740.

176. Kroon, J. M. *et al.*, Nanocrystalline dye-sensitized solar cells having maximum performance. *Progr. Photovolt.*, 2007, **15**, 1–18.

177. Kuang, D. B., Klein, C., Ito, S., Moser, J. E., Humphry-Baker, R., Zakeeruddin, S. M. and Gratzel, M., High molar extinction coefficient ion-coordinating ruthenium sensitizer for efficient and stable mesoscopic dye-sensitized solar cells. *Adv. Functional Mater.*, 2007, **17**, 154–160.

178. Gratzel, M., The advent of mesoscopic injection solar cells. *Progr. Photovoltaics*, 2006, **14**, 429–442.

179. Kuang, D. B. *et al.*, High molar extinction coefficient heteroleptic ruthenium complexes for thin film dye-sensitized solar cells. *J. Am. Chem. Soc.*, 2006, **128**, 4146–4154.

180. Wang, P., Klein, C., Humphry-Baker, R., Zakeeruddin, S. M. and Gratzel, M., Stable $>= 8\%$ efficient nanocrystalline dye-sensitized solar cell based on an electrolyte of low volatility. *Appl. Phys. Lett.*, 2005, **86**, 123508.

181. Wang, P., Zakeeruddin, S. M., Humphry-Baker, R. and Gratzel, M., A binary ionic liquid electrolyte to achieve $>= 7\%$ power conversion efficiencies in dye-sensitized solar cells. *Chem. Mater.*, 2004, **16**, 2694–2696.

182. Gratzel, M., Conversion of sunlight to electric power by nanocrystalline dye-sensitized solar cells. *J. Photochem. Photobiol A – Chem.*, 2004, **164**, 3–14.

183. Wang, P., Zakeeruddin, S. M., Humphry-Baker, R., Moser, J. E. and Gratzel, M., Molecular-scale interface engineering of TiO_2 nanocrystals: Improving the efficiency and stability of dye-sensitized solar cells. *Adv. Mater.*, 2003, **15**, 2101–2106.

184. Wang, P., Zakeeruddin, S. M., Comte, P., Charvet, R., Humphry-Baker, R. and Gratzel, M., Enhance the performance of dye-sensitized solar cells by co-grafting amphiphilic sensitizer and hexadecylmalonic acid on TiO_2 nanocrystals. *J. Phys. Chem.*, 2003, **B107**, 14336–14341.

185. Wang, P., Zakeeruddin, S. M., Moser, J. E., Nazeeruddin, M. K., Sekiguchi, T. and Gratzel, M., A stable quasi-solid-state dye-sensitized solar cell with an amphiphilic ruthenium sensitizer and polymer gel electrolyte. *Nature Mater.*, 2003, **2**, 402–407.

186. Kay, A. and Gratzel, M., Dye-sensitized core-shell nanocrystals: Improved efficiency of mesoporous tin oxide electrodes coated with a thin layer of an insulating oxide. *Chem. Mater.*, 2002, **14**, 2930–2935.

187. Burke, A., Schmidt-Mende, L., Ito, S. and Gratzel, M., A novel blue dye for near-IR dye-sensitised solar cell applications. *Chem. Commun.*, 2007, 234–236.

188. Clifford, J. N., Palomares, E., Nazeeruddin, M. K., Gratzel, M. and Durrant, J. R., Dye dependent regeneration dynamics in dye sensitized nanocrystalline solar cells: Evidence for the formation of a ruthenium bipyridyl cation/iodide intermediate. *J. Phys. Chem.*, 2007, **C111**, 6561–6567.

189. De Angelis, F. *et al.*, Controlling phosphorescence color and quantum yields in cationic iridium complexes: A combined experimental and theoretical study. *Inorg. Chem.*, 2007, **46**, 5989–6001.

190. De Angelis, F., Fantacci, S., Selloni, A., Gratzel, M. and Nazeeruddin, M. K., Influence of the sensitizer adsorption mode on the open-circuit potential of dye-sensitized solar cells. *Nano Lett.*, 2007, **7**, 3189–3195.

191. Fabregat-Santiago, F., Bisquert, J., Palomares, E., Otero, L., Kuang, D. B., Zakeeruddin, S. M. and Gratzel, M., Correlation between photovoltaic performance and impedance spectroscopy of dye-sensitized solar cells based on ionic liquids. *J. Phys. Chem.*, 2007, **C111**, 6550–6560.

192. Poplin, J. H. *et al.*, Sensor technologies based on a cellulose supported platform. *Chem. Commun.*, 2007, 2025–2027.

193. Gratzel, M., Molecular photovoltaics that mimic photosynthesis. *Pure Appl. Chem.*, 2001, **73**, 459–467.

194. Argazzi, R., Bignozzi, C. A., Heimer, T. A. and Meyer, G. J., Remote interfacial electron transfer from supramolecular sensitizers. *Inorg. Chem.*, 1997, **36**, 2–3.

195. Bonchio, M., Carofiglio, T., Carraro, M., Fornasier, R. and Tonellato, U., Efficient sensitized photooxygenation in water by a porphyrin-cyclodextrin supramolecular complex. *Org. Lett*, 2002, **4**, 4635–4637.

196. Bignozzi, C. A., Schoonover, J. R. and Scandola, F., Molecular level artificial photosynthetic materials. *Progr. Inorg. Chem.*, 1997, **44**, 1–95.

197. Haque, S. A., Handa, S., Peter, K., Palomares, E., Thelakkat, M. and Durrant, J. R., Supermolecular control of charge transfer in dye-sensitized nanocrystalline TiO_2 films: Towards a quantitative structure–function relationship. *Angew. Chemie – Int. Ed.*, 2005, **44**, 5740–5744.

198. Kalyanasundaram, K. and Gratzel, M., Applications of functionalized transition metal complexes in photonic and optoelectronic devices. *Coord. Chem. Rev.*, 1998, **177**, 347–414.

199. Argazzi, R., Bignozzi, C. A., Heimer, T. A., Castellano, F. N. and Meyer, G. J., Enhanced spectral sensitivity from ruthenium(II) polypyridyl based photovoltaic devices. *Inorg. Chem.*, 1994, **33**, 5741–5749.

200. Kohle, O., Gratzel, M., Meyer, A. F. and Meyer, T. B., The photovoltaic stability of bis(isothiocyanato)ruthenium(II)-bis-2,2′-bipyridine-4,4′-dicarboxylic acid and related sensitizers. *Adv. Mat.*, 1997, **9**, 904–910.

201. Araki, K., Losco, P., Engelmann, F. M., Winnischofer, H. and Toma, H. E., Modulation of vectorial energy transfer in the tetrakis[tris(bipyridine)ruthenium(II)]porphyrinate zinc complex. *J. Photochem. Photobiol. A – Chemistry*, 2001, **142**, 25–30.

202. Koehorst, R. B. M., Boschloo, G. K., Savenije, T. J., Goossens, A. and Schaafsma, T. J., Spectral sensitization of TiO_2 substrates by monolayers of porphyrin heterodimers. *J. Phys. Chem.*, 2000, **B104**, 2371–2377.

203. Fungo, F., Otero, L., Bosarelli, C. D., Durantini, E. N., Silber, J. J. and Sereno, L., Photocurrent generation in thin SnO_2 nanocrystalline semiconductor film electrodes from photoinduced charge-separation state in porphyrin-C_{60} Dyad. *J. Phys. Chem.*, 2002, **B106**, 4070–4078.

204. Odobel, F. *et al.*, Porphyrin dyes for TiO_2 sensitization. *J. Mater. Chem.*, 2003, **13**, 502–510.

205. Viseu, T. M. R., Hungerford, G. and Ferreira, M. I. C., Optical and photophysical studies on porphyrin doped TiO_2 matrixes. *J. Phys. Chem.*, 2002, **B106**, 1853–1861.

206. Monk, P. M. S., Mortimer, R. J. and Rosseinsky, D. R., *Electrochromism*, VCH, Weinheim, 1995.

207. Biancardo, M., Argazzi, R. and Bignozzi, C. A., Electrochromic devices based on wide band-gap nanocrystalline semiconductors functionalized with mononuclear charge transfer compounds. *Displays*, 2006, **27**, 19–23.

208. Biancardo, M., Argazzi, R. and Bignozzi, C. A., Solid-state photochromic device based on nanocrystalline TiO_2 functionalized with electron donor–acceptor species. *Inorg. Chem.*, 2005, **44**, 9619–9621.

209. Biancardo, M., Schwab, P. F. H., Argazzi, R. and Bignozzi, C. A., Electrochromic devices based on binuclear mixed valence compounds adsorbed on nanocrystalline semiconductors. *Inorg. Chem.*, 2003, **42**, 3966–3968.

210. Nogueira, A. F., Toma, S. H., Vidotti, M., Formiga, A. L. B., de Torresi, S. I. C. and Toma, H. E., A highly efficient redox chromophore for simultaneous application in a photoelectrochemical dye sensitized solar cell and electrochromic devices. *New J. Chem.*, 2005, **29**, 320–324.

211. Bonhote, P., Moser, J. E., Humphry-Baker, R., Vlachopoulos, N., Zakeeruddin, S. M., Walder, L., and Gratzel, M., Long-lived photoinduced charge separation and redox-type photochromism on mesoporous oxide films sensitized by molecular dyads. *J. Am. Chem. Soc.*, 1999, **121**, 1324–1336.

212. Campus, F., Bonhote, P., Gratzel, M., Heinen, S. and Walder, L., Electrochromic devices based on surface-modified nanocrystalline TiO_2 thin-film electrodes. *Solar Energy Mater. Solar Cells*, 1999, **56**, 281–297.

213. Cummins, D., Boschloo, G., Ryan, M., Corr, D., Rao, S. N. and Fitzmaurice, D., Ultrafast electrochromic windows based on redox-chromophore modified nanostructured semiconducting and conducting films. *J. Phys. Chem.*, 2000, **B104**, 11449–11459.

214. Schwab, P. F. H., Diegoli, S., Biancardo, M. and Bignozzi, C. A., Novel Ru-dioxolene complexes as potential electrochromic materials and NIR dyes. *Inorg. Chem.*, 2003, **42**, 6613–6615.

215. Pichot, F., Beck, J. H. and Elliott, C. M., A series of multicolor electrochromic ruthenium(II) trisbipyridine complexes: Synthesis and electrochemistry. *J. Phys. Chem.*, 1999, **A103**, 6263–6267.

216. Garcia-Canadas, J., Meacham, A. P., Peter, L. M. and Ward, M. D., Electrochromic switching in the visible and near IR with a Ru-dioxolene complex adsorbed on a nanocrystalline SnO_2 electrode. *Electrochem. Comm.*, 2003, **5**, 416–420.

217. Surca, A., Orel, B., Pihlar, B. and Bukovec, P., *J. Electroanal. Chem.*, 1996, **408**, 83–88.

218. Granqvist, C. G., *Handbook of Inorganic Electrochromic Materials*, Elsevier, Oxford, 1995.

219. Fonseca, C. N. P., De Paoli, M. A. and Gorenstein, A., *Sol. Energy Mater. Sol. Cells*, 1994, **33**, 73–81.

220. Orlov, A. O. *et al.*, Experimental demonstration of clocked single-electron switching in quantum-dot cellular automata. *Appl. Phys. Let.*, 2000, **77**, 295–297.

221. Amlani, I., Orlov, A. O., Toth, G., Bernstein, G. H., Lent, C. S. and Snider, G. L., Digital logic gate using quantum-dot cellular automata. *Science*, 1999, **284**, 289–291.

222. Collier, C. P. *et al.*, Electronically configurable molecular-based logic gates. *Science*, 1999, **285**, 391–394.

223. Luo, Y. *et al.*, Two-dimensional molecular electronics circuits. *Chemphyschem*, 2002, **3**, 519–522.

224. Ami, S., Hliwa, M. and Joachim, C., Molecular 'OR' and 'AND' logic gates integrated in a single molecule. *Chem. Phys. Lett.*, 2003, **367**, 662–668.

225. O'Brien, J. L., Pryde, G. J., White, A. G., Ralph, T. C. and Branning, D., Demonstration of an all-optical quantum controlled-NOT gate. *Nature*, 2003, **426**, 264–267.

226. Saghatelian, A., Volcker, N. H., Guckian, K. M., Lin, V. S. Y. and Ghadiri, M. R., DNA-based photonic logic gates: AND, NAND, and INHIBIT. *J. Am. Chem. Soc.*, 2003, **125**, 346–347.

227. Ball, P., Chemistry meets computing. *Nature*, 2000, **406**, 118–120.

228. Weizmann, Y., Elnathan, R., Lioubashevski, O. and Willner, I., Endonuclease-based logic gates and sensors using magnetic force-amplified readout of DNA scission on cantilevers. *J. Am. Chem. Soc.*, 2005, **127**, 12666–12672.

229. Raymo, F. M., Digital processing and communication with molecular switches. *Adv. Mat.*, 2002, **14**, 401–409.

230. Auvray, S., Derycke, V., Goffman, M., Filoramo, A., Jost, O. and Bourgoin, J. P., Chemical optimization of self-assembled carbon nanotube transistors. *Nano Lett.*, 2005, **5**, 451–455.

231. Pease, A. R., Jeppesen, J. O., Stoddart, J. F., Luo, Y., Collier, C. P. and Heath, J. R., Switching devices based on interlocked molecules. *Acc. Chem. Res.*, 2001, **34**, 433–444.

232. Li, C. *et al.*, Fabrication approach for molecular memory arrays. *Appl. Phys. Lett.*, 2003, **82**, 645–647.

233. Tour, J. M., Molecular electronics. Synthesis and testing of components. *Acc. Chem. Res.*, 2000, **33**, 791–804.

234. Joachim, C., Gimzewski, J. K. and Aviram, A., Electronics using hybrid-molecular and mono-molecular devices. *Nature*, 2000, **408**, 541–548.

235. Collier, C. P., Jeppesen, J. O., Luo, Y., Perkins, J., Wong, E. W., Heath, J. R. and Stoddart, J. F., Molecular-based electronically switchable tunnel junction devices. *J. Am. Chem. Soc.*, 2001, **123**, 12632–12641.

236. Tian, H., Qin, B., Yao, R. X., Zhao, X. L. and Yang, S. J., A single photochromic molecular switch with four optical outputs probing four inputs. *Adv. Mater.*, 2003, **15**, 2104–2109.

237. Rocha, R. C., Rein, F. N. and Toma, H. E., Ruthenium and iron complexes with benzotriazole and benzimidazole derivatives as simple models for proton-coupled electron transfer systems. *J. Braz. Chem. Soc.*, 2001, **12**, 234–242.

238. Wagner, R. W. and Lindsey, J. S., A molecular photonic wire. *J. Am. Chem. Soc.*, 1994, **116**, 9759–9760.

239. James, D. K. and Tour, J. M., Molecular wires: from design to properties. *Topics Cur. Chem.*, 2005, **257**, 33–62.

240. Wang, C. S., Batsanov, A. S., Bryce, M. R., Ashwell, G. J., Urasinska, B., Grace, I. and Lambert, C. J., Electrical characterization of 7 nm long conjugated molecular wires: experimental and theoretical studies. *Nanotechnology*, 2007, **18**, 1–8.

241. Weiss, E. A., Ahrens, M. J., Sinks, L. E., Gusev, A. V., Ratner, M. A. and Wasielewski, M. R., Making a molecular wire: Charge and spin transport through para-phenylene oligomers. *J. Am. Chem. Soc.*, 2004, **126**, 5577–5584.

242. Ashwell, G. J., Tyrrell, W. D., Urasinska, B., Wang, C. S. and Bryce, M. R., Organic rectifying junctions from an electron-accepting molecular wire and an electron-donating phthalocyanine. *Chem. Commun.*, 2006, 1640–1642.

243. Biancardo, M., Bignozzi, C., Hugh, D. C. and Redmond, G., A potential and ion switched molecular photonic logic gate. *Chem. Commun.*, 2005, 3918–3920.

244. Stojanovic, M. N., Mitchell, T. E. and Stefanovic, D., Deoxyribozyme-based logic gates. *J. Am. Chem. Soc.*, 2002, **124**, 3555–3561.

245. Zauner, K. P. and Conrad, M., Enzymatic computing. *Biotechnol. Progr.*, 2001, **17**, 553–559.

246. Chen, Y. *et al.*, Nanoscale molecular-switch crossbar circuits. *Nanotechnology*, 2003, **14**, 462–468.

247. Heinrich, A. J., Lutz, C. P., Gupta, J. A. and Eigler, D. M., Molecule cascades. *Science*, 2002, **298**, 1381–1387.

248. Lent, C. S., Isaksen, B. and Lieberman, M., Molecular quantum-dot cellular automata. *J. Am. Chem. Soc.*, 2003, **125**, 1056–1063.

249. Allwood, D. A., Xiong, G., Faulkner, C. C., Atkinson, D., Petit, D. and Cowburn, R. P., Magnetic domain-wall logic. *Science*, 2005, **309**, 1688–1692.

250. Allwood, D. A., Xiong, G., Cooke, M. D., Faulkner, C. C., Atkinson, D. and Cowburn, R. P., Characterization of submicrometer ferromagnetic NOT gates. *J. Appl. Phys.*, 2004, **95**, 8264–8270.

251. Cowburn, R. P., Magnetic nanodots for device applications. *J. Magn. Magn. Mater.*, 2002, **242**, 505–511.

252. Cowburn, R. P. and Welland, M. E., Room temperature magnetic quantum cellular automata. *Science*, 2000, **287**, 1466–1468.

253. Matsui, J., Mitsuishi, M., Aoki, A. and Miyashita, T., Optical logic operation based on polymer Langmuir–Blodgett-film assembly. *Angew. Chem. – Int. Ed.*, 2003, **42**, 2272–2275.

254. Straight, S. D. *et al.*, All-photonic molecular XOR and NOR logic gates based on photochemical control of fluorescence in a fulgimide-porphyrin-dithienylethene triad. *Adv. Funct. Mater.*, 2007, **17**, 777–785.

255. Andreasson, J. *et al.*, All-photonic molecular half-adder. *J. Am. Chem. Soc.*, 2006, **128**, 16259–16265.

256. Straight, S. D. *et al.*, Molecular AND and INHIBIT gates based on control of porphyrin fluorescence by photochromes. *J. Am. Chem. Soc.*, 2005, **127**, 9403–9409.

257. Magri, D. C., Brown, G. J., McClean, G. D. and de Silva, A. P., Communicating chemical congregation: A molecular AND logic gate with three chemical inputs as a 'lab-on-a-molecule' prototype. *J. Am. Chem. Soc.*, 2006, **128**, 4950–4951.

258. Uchiyama, S., McClean, G. D., Iwai, K. and de Silva, A. P., Membrane media create small nanospaces for molecular computation. *J. Am. Chem. Soc.*, 2005, **127**, 8920–8921.

259. Creager, S. E. and Radford, P. T., Electrochemical reactivity at redox-molecule-based nanoelectrode ensembles. *J. Electroanal. Chem.*, 2001, **500**, 21–29.

260. Ashton, P. R. *et al.*, Acid-base controllable molecular shuttles. *J. Am. Chem. Soc.*, 1998, **120**, 11932–11942.

261. Ashton, P. R. *et al.*, A photochemically driven molecular-level abacus. *Chem. – A Eur. J.*, 2000, **6**, 3558–3574.

262. Nazeeruddin, M. K. *et al.*, Conversion of light to electricity by cis-X2bis(2,2′-Bipyridyl-4,4′-dicarboxylate)ruthenium(II) charge-transfer sensitizers (X = Cl–, Br–, I–, CN–, and SCN–) on nanocrystalline TiO_2 electrodes. *J. Am. Chem. Soc.*, 1993, **115**, 6382–6390.

263. Conrad, M. and Zauner, K. P., *Molecular Computing*, MIT Press, Boston, 2003.